https://doi.org/10.5194/egusphere-2023-2307
Preprint. Discussion started: 24 October 2023

Climate feedbacks with latitude derived from climatological data and theory

Philip Goodwin[1], Richard G. Williams[2], Paulo Ceppi[3,4], B. B. Cael[5]

[1]School of Ocean and Earth Science, University of Southampton, SO14 3ZH, UK
[2]Department of Earth, Ocean and Ecological Sciences, School of Environmental Sciences, University of Liverpool, Liverpool, L69 3GP UK
[3]Grantham Institute, Imperial College London, London, SW7 2AZ, UK
[4]Department of Physics, Imperial College London, London, SW7 2AZ, UK
[5]Ocean Biogeosciences, National Oceanography Centre, European Way, Southampton, SO14 3ZH, UK

Correspondence to: Philip Goodwin (p.a.goodwin@soton.ac.uk)

Abstract. Most current methods for evaluating climate feedbacks utilise variation with time in Earth's energy balance and surface temperatures, either from observations or Earth system model perturbation experiments. This study presents a new semi-empirical evaluation of Earth's climate feedbacks at equilibrium, constrained instead by variation with latitude in recent mean climatology. Latitudinally binned surface temperature and outgoing radiation climatology provides a first order net climate feedback estimate $\lambda = -1.3 \pm 0.1$ Wm^{-2}K^{-1}, but this does not isolate the temperature influence on outgoing radiation from other factors. To isolate the surface temperature influence: First, we derive approximated functional relations for outgoing shortwave and longwave radiation in terms of surface temperature, surface relative humidity, fractional cloud amount, tropopause height and incident solar radiation. Second, we use observations of current zonal-mean climatology to constrain the relations and apply calculus to evaluate non-cloud climate feedbacks with latitude, including the Planck, water vapour-lapse rate and surface albedo. Our novel climatology-based evaluations of climate feedbacks weighted by the recent warming pattern, when combined with a recent estimate of cloud feedback from multiple lines of evidence, implies a global mean total net climate feedback $\lambda = -1.1$ (-0.8 to -1.4 at 66% range) Wm^{-2}K^{-1} consistent with recent assessments of the literature. Our latitudinal method to constrain non-cloud climate feedback is independent of previous temporal approaches, using different observational lines of evidence, and so our method complements existing methods to help constrain climate feedback and climate sensitivity.

1 Introduction

Recent climatology reveals significant latitudinal variation in the annual- and zonal-mean values of both surface temperature and outgoing radiation at the top-of-the-atmosphere (Fig. 1, black). Current anthropogenic emissions of greenhouse gasses and aerosols are inducing a radiative forcing perturbation, δF in Wm^{-2}, and altering the top-of-the-atmosphere energy balance (e.g. IPCC, 2021). The climate feedback, λ in Wm^{-2}K^{-1}, expresses how the Earth's surface temperature change will restore the climate system's top-of-atmosphere energy balance following a radiative forcing perturbation, δF (e.g. Sherwood et al., 2020).

https://doi.org/10.5194/egusphere-2023-2307
Preprint. Discussion started: 24 October 2023

Evaluating climate feedback is a central goal of climate science, as the feedback determines the level of surface warming that will eventually occur to re-balance anthropogenic greenhouse forcing once ocean heat uptake ceases. The current Intergovernmental Panel on Climate Change Assessment Report 6 (IPCC, 2021) estimate retains significant uncertainty in climate feedback processes (Fig. 2, blue for AR6, orange and red for CMIP5 and CMIP6; Table 1), as do other estimates from multiple lines of evidence (e.g. Sherwood et al., 2020: Table 1). Climate feedback is evaluated in global climate models using finite perturbation experiments, often by raising atmospheric CO_2 to 4 times the preindustrial level and comparing simulated output to a control run (e.g. Soden et al. 2008; Zelinka et al., 2020). Observational estimates of climate feedback consider the climate's temporal responses to anthropogenic forcing (e.g. Otto et al., 2013), or the climate's temporal variability (e.g. Dessler, 2013).

The climate feedback, λ, can be evaluated by ascertaining how the outgoing shortwave and longwave radiation at the top of the atmosphere vary with changes in surface temperature. This differential is usually evaluated from temporal changes in local and global climate, which amounts to variation in surface temperature and outgoing radiation of order 1 K and 1 Wm^{-2} in historical observations (e.g. Morice et al., 2021) and up to order 10 K and 10 Wm^{-2} in model perturbation experiments (e.g. Zelinka et al., 2020) respectively.

Instead, this study presents a novel method to evaluate climate feedback drawing upon much larger temperature variations with latitude, reaching order 70 K (Jones et al., 1999), and significant variation in outgoing shortwave and longwave radiation with latitude, reaching order 70 Wm^{-2} (Loeb et al., 2018) in current mean climatology (Fig. 1, black). To evaluate climate feedback using this latitudinal variation in mean climatology, one first must extract how much of the total variation in the outgoing shortwave and longwave radiation with latitude relates to surface temperature, and how much relates to other climate properties. Section 1.1 now explores the existing methodologies for evaluating climate feedback using temporal climate variation, while section 1.2 introduces the new methodology based on latitudinal climate variation. This new methodology is applied to evaluate both clear-sky feedbacks (when clouds are absent) and non-cloud feedbacks (when clouds are present in their climatological all-sky state but there is no change to cloud amount, altitude or type with perturbation).

1.1 Approaches for evaluating climate feedback from temporal variation in climate

The challenge is to evaluate the climate feedback due to some process X, λ_X in $Wm^{-2}K^{-1}$, which is defined in the general sense as minus the partial derivative of outgoing shortwave and longwave radiation with respect to surface temperature change due to the response to process X,

$$\lambda_X = -\frac{\partial[S_{out}+L_{out}]}{\partial T_S}\Big|_{\delta X} = -\frac{\partial[S_{out}+L_{out}]}{\partial X}\frac{\partial X}{\partial T_S}, \quad (1)$$

https://doi.org/10.5194/egusphere-2023-2307
Preprint. Discussion started: 24 October 2023

where L_{out} and S_{out} are the outgoing longwave radiation and shortwave radiation at the top of the atmosphere in Wm^{-2}; T_S is the surface temperature in K; and X is some property of the climate system that both has a dependence on surface temperature and upon which outgoing radiation is dependent. The variables T_S, L_{out} and S_{out} can be chosen to refer to either global spatially averaged quantities, if λ_X is evaluated as a global mean only, or spatially varying quantities, if spatial information in λ_X is sought. This goal of evaluating eq. (1) is usually achieved by considering the temporal variations, either in numerical model perturbation experiments or from observations of historical climate change, where a radiative forcing, δF in Wm^{-2}, is applied. In this case, a small imposed δF is balanced over time by the Earth's energy imbalance, δN in Wm^{-2}, and the longwave and shortwave radiative responses from elevated surface temperatures,

$$\delta F - \delta N = \frac{\delta[L_{out}+S_{out}]}{\delta T_S}\delta T_s = -\lambda_{total}\delta T_S \quad (2)$$

where δ signifies the change over time in a quantity between an initial state and a perturbed state; and λ_{total} is the total net feedback from all processes in Wm^{-2}K^{-1}. In these temporal perturbation experiments the finite change in outgoing radiation per unit finite change in temperature, $\frac{\delta[L_{out}+S_{out}]}{\delta T_S}$, term in eq. (2) is used as an approximation for the partial derivative, $\frac{\partial[L_{out}+S_{out}]}{\partial T_S}$, term in eq. (1), to evaluate climate feedback. Constraining the changes over time in δF, δN and δT_s in numerical experiments or historical observations then reveals the value of $\frac{\delta[L_{out}+S_{out}]}{\delta T_S}$, and therefore λ, eq. (2). Methods that evaluate separate climate feedbacks within finite perturbation experiments (e.g. Soden et al., 2008; Zelinka et al., 2020) then assume the overall climate feedback is composed of individual climate feedbacks from different processes that are linearly separable:

$$\lambda_{total} \approx \sum_X \lambda_X \quad (3)$$

such that eq. (1) may be approximated via small changes, δ, rather than partial derivatives, ∂:

$$\lambda_X \approx -\frac{\delta[L_{out}+S_{out}]}{\delta X}\frac{\delta X}{\delta T_S}. \quad (4)$$

Any method that seeks to evaluate separate climate feedback terms from different processes, λ_X (eq. 1), using finite perturbations to the system, $\delta T_S \nrightarrow 0$ and $\delta X \nrightarrow 0$, must ultimately make the linearly separable assumption, eq. (3), since $\frac{\delta[L_{out}+S_{out}]}{\delta T_S}$ in eq. (4) only becomes equal to $\frac{\partial[L_{out}+S_{out}]}{\partial X}$ in eq. (1) in the general case when perturbations are infinitesimal, $\delta T_S \to 0$ and $\delta X \to 0$. For example, in one analysis of CMIP6 models from a 4xCO_2 perturbation experiment (Zelinka et al., 2020, see Supplementary Information therein) the discrepancy between the sum of individual climate feedbacks, $\sum_X \lambda_X$, and the net climate feedback, λ, ranges from -0.25 Wm^{-2}K^{-1} to +0.37 Wm^{-2}K^{-1}, eq. (3).

There are approximations in the standard method for evaluating λ_X, eq. (4), using the differences over time between some initial and perturbed state. Firstly, uncertainty is introduced when evaluating λ_X from eq. (4) using small surface temperature perturbations over time, δT_S, as there is a low signal-to-noise ratio. However, uncertainty is also introduced when using large surface temperature perturbations over time, δT_S, because the assumption of linearly separable feedbacks, eq. (3), only strictly holds for infinitesimal perturbations (e.g. introducing the error term in the net feedback in Zelinka et al., 2020). Secondly,

https://doi.org/10.5194/egusphere-2023-2307
Preprint. Discussion started: 24 October 2023

when applying eq. (4) to numerical model experiments, some additional analysis must be conducted to establish how the numerical models relate to the real climate system, for example via emergent constraints (Cox et al., 2018).

In addition, climate feedback terms have also been evaluated from data-based approaches, for example by considering the short timescale variability in outgoing radiation and temperature (Dessler, 2013) or by considering the time evolutions of historic surface warming, radiative forcing and ocean heat uptake (e.g. Otto et al., 2013; Goodwin and Cael, 2021; Cael et al., 2023). These observation-based methods evaluate climate feedbacks from eqs. (2) to (4), by considering the historic observed changes over time in δT_S, δF, δN and $\delta[L_{out} + S_{out}]$. However, the magnitude of historic changes in δT_S over time is relatively small, while uncertainty in historic changes over time in δF, δN and $\delta[L_{out} + S_{out}]$ is relatively large (e.g. IPCC, 2021; Sherwood et al., 2020), leading to a potentially low signal-to-noise ratio. Also, the method here differs by using latitudinal variation in observations to estimate the equilibrium climate feedback, where many previous methods (e.g. Otto et al., 2013; Cael et al., 2023) use temporal variation in observations to calculate the current effective climate feedback. Due to the long timescale of some relevant processes (for example the evolving pattern of sea surface temperature warming), the current state can have a larger climate feedback, and smaller climate sensitivity, than is expected at equilibrium (e.g. compare Otto et al., 2013 and Cael et al., 2023 to Sherwood et al., 2020).

1.2 A new approach for evaluating climate feedback from latitudinal variation in mean climatology

Now consider how variation *with latitude* in surface temperature and outgoing radiation can be used to constrain the net climate feedback, λ, and the separate climate feedbacks for individual processes, $\lambda_X = -\frac{\partial[L_{out}+S_{out}]}{\partial T_S}\Big|_{\delta X}$: eq. (1). Firstly, by simply plotting the climatological zonal-mean outgoing radiation against surface temperature for the period July 2005 to June 2015, we find $\frac{\delta[L_{out}+S_{out}]}{\delta T_S} = 1.30 \pm 0.06$ Wm^{-2}K^{-1} (Fig. 1). If we again make the assumption that $\frac{\delta[L_{out}+S_{out}]}{\delta T_S} \approx \frac{\partial[L_{out}+S_{out}]}{\partial T_S}$, then a first-order estimate of net climate feedback of $\lambda_{total} = -1.30 \pm 0.06$ Wm^{-2}K^{-1} is obtained, eq. (2). This latitudinal estimate is in excellent agreement with previous temporal variation-based estimates, for example the best estimate from Sherwood et al. (2020) of $\lambda_{total} = -1.30$ Wm^{-2}K^{-1} (Table 1).

At first glance, and given the close agreement with temporal estimates (Table 1), this latitudinal estimate of net climate feedback, λ_{total}, (Fig. 1, red) appears robust: 93% of the observed variance in outgoing radiation data is explained by surface temperature; the data spans order 70 K in temperature variation and 70 Wm^{-2} in outgoing radiation variation and so has a high signal to noise ratio; and the uncertainty in the gradient of the best fit is small (Fig. 1). However, some portion of the variance in outgoing radiation may be linked to other factors that co-varied spatially with temperature over the diagnosed period from July 2005 to June 2015, but would not co-vary in response to a temperature perturbation, causing $\frac{\delta[L_{out}+S_{out}]}{\delta T_S} \not\approx \frac{\partial[L_{out}+S_{out}]}{\partial T_S}$. Such factors could include latitudinal variation in incident solar radiation, latitudinal changes in albedo due to the solar zenith

https://doi.org/10.5194/egusphere-2023-2307
Preprint. Discussion started: 24 October 2023

angle, or latitudinal variation in the height of the tropopause. Also, this linear gradient estimate (Fig. 1) does not allow the possibility for λ_{total} to vary spatially, nor does it weight the different spatial λ_{total} values to reach a global mean. There is no mechanism for calculating the individual climate feedbacks from different processes, λ_X.

The goal here is to constrain net climate feedback, λ_{total} and climate feedbacks from individual component processes, λ_X, with latitude, and as a global mean, through the application of theory and observed recent climatology of the latitudinal variation in annual- and zonal-mean climatological quantities. The challenge for the theory is to extract the components of changes in $L_{out} + S_{out}$ that arise due to changes in T_S from the components that change due to other factors: i.e. to calculate $\frac{\partial[L_{out}+S_{out}]}{\partial T_S}$ and not $\frac{\delta[L_{out}+S_{out}]}{\delta T_S}$.

As well as the high signal to noise ratio arising from large spatial variation in ΔT_S and $\Delta[L_{out} + S_{out}]$ (Fig. 1), the recent latitudinal climatology method for constraining climate feedback presented here (Sections 2 to 6) does not require evaluation of the radiative forcing, δF, or Earth's energy imbalance, δN, and so large uncertainties in these quantities for temporal evaluation (IPCC, 2021) does not affect the constraints achieved. A further benefit of the latitudinal climate variation approach is that the climate feedbacks for different processes, λ_X, may be evaluated without needing to invoke the linearly-separable feedbacks assumption, eq. (3).

The different feedback processes, λ_X, evaluated include the Planck feedback with constant specific humidity; temperature feedback with constant relative humidity; the combined water vapour-lapse rate feedback; and the surface albedo feedback. These feedbacks are evaluated for clear-sky conditions, without clouds, and all-sky conditions, where clouds are present but do not change under perturbation. Feedbacks from changes in cloud amount, cloud altitude or cloud type are not calculated in this study as the focus is on extracting information from latitudinal variation in the observed climatological mean, and this information does not reveal how clouds change over time in response to forcing. The annual- and zonal-mean climatological quantities used to constrain climate feedbacks in this study include: surface temperatures, T_S (CRUTEM and HadCRUT5 datasets: Jones et al., 1999; Morice et al., 2021); outgoing longwave and shortwave radiation, L_{out} and S_{out} (CERES EBAF v4.1 dataset: Loeb et al., 2018), incident solar radiation, R_{solar} (calculated from geometry after Hartmann, 1994); cloud amount fraction, f_{CA} (CLARA v2.1 dataset: Karlsson et al., 2021); surface relative humidity, H_{rel} (ERA5 reanalysis: Hersbach et al., 2018); the height of the tropopause, z_{trop} (empirically constrained bilinear model: Mateus et al., 2022); and latitude, ϕ.

Section 2 explores the relations for climate feedback in the general case drawing upon how observations of the recent climatology vary with latitude. Section 3 then evaluates the Planck feedback at constant specific humidity, the water vapour-lapse rate (WVLR) feedback and the Planck feedback under constant specific humidity by applying these relations for longwave radiation under clear-sky, cloudy-sky and all-sky conditions, and using approximate functional relations constrained

https://doi.org/10.5194/egusphere-2023-2307
Preprint. Discussion started: 24 October 2023

by observations. Section 4 evaluates the surface albedo feedback by applying these relations for shortwave radiation under clear-sky, cloudy-sky and all-sky conditions, and using approximate functional relations constrained by observations. Section 5 then calculates the implied total net climate feedback from all processes by combining the non-cloud climate feedbacks evaluated here with a recent independent estimate of cloud feedback (Sherwood et al., 2020). Section 6 discusses the results of the study in the context of previous methods to constrain the climate feedback (Fig. 2; Table 1) and a kernel decomposition of zonal climate feedbacks from 15 CMIP6 models (Appendix A).

2 Relations for climate feedback constrained by annual- and zonal-mean climatology

At the top of the atmosphere, the outgoing radiation, $R_{out,i}(\phi)$ in Wm^{-2}, involves the sum of the outgoing longwave radiation $L_{out,i}(\phi)$ and the outgoing solar radiation $S_{out,i}(\phi)$, which are each related respectively to the surface temperature, $T_s(\phi)$, via the emissivity, $\varepsilon_i(\phi)$, and the incoming solar radiation, $R_{solar}(\phi)$ in Wm^{-2} via the albedo, $\alpha_i(\phi)$,

$$R_{out,i}(\phi) = L_{out,i}(\phi) + S_{out,i}(\phi) = \varepsilon_i(\phi)\sigma T_S^4(\phi) + \alpha_i(\phi)R_{solar}(\phi) \quad (5)$$

where annual and zonal means are applied for latitude ϕ and cloud-state i (clear or cloudy sky), $\sigma = 5.67 \times 10^8$ Wm^{-2}K^{-4} is the Stefan-Boltzmann constant, $T_S^4(\phi)$ is evaluated raised to the 4th power prior to annual- and zonal-averaging, and ε_i is the bulk emissivity and α_i is the albedo under cloud-state i. ε_i and α_i are defined (Goodwin and Williams, 2023),

$$\varepsilon_i(\phi) = \int_t^{t+n\Delta t} \frac{L_{out,i}(\phi,t')}{\sigma T_S^4(\phi,t')} dt' \Big/ \int_t^{t+n\Delta t} dt' \quad (6a)$$

and

$$\alpha_i(\phi) = \int_t^{t+n\Delta t} \frac{R_{in}(\phi,t')}{S_{out,i}(\phi,t')} dt' \Big/ \int_t^{t+n\Delta t} dt' \quad (6b)$$

where $n\Delta t$ is some integer number of years over which the climatological period is defined, and all quantities are evaluated at latitude ϕ, but may not be a simple function of latitude.

The emissivity under all-sky conditions is equal to the cloudy sky fraction multiplied by the cloudy-sky emissivity plus the clear sky amount multiplied by the clear-sky emissivity,

$$\varepsilon_{AllSky}(\phi) = f_{CA}(\phi)\varepsilon_{CloudySky}(\phi) + [1 - f_{CA}(\phi)]\varepsilon_{ClearSky}(\phi) \quad (7a)$$

where $f_{CA}(\phi)$ is the fraction of cloud amount at latitude ϕ, expressed as a fraction between 0 and 1 and all terms are separately evaluated as an annual and zonal-mean. Similarly, the albedo under all-sky conditions is equal to the fraction of solar radiation incident on a cloudy sky multiplied by the cloudy-sky albedo plus the fraction of solar radiation that is incident on a clear sky multiplied by the clear-sky albedo,

$$\alpha_{AllSky}(\phi) = f_{CI}(\phi)\alpha_{CloudySky}(\phi) + [1 - f_{CI}(\phi)]\alpha_{ClearSky}(\phi) \quad (7b)$$

where $f_{CI}(\phi)$ is the annual- and zonal-mean fraction of solar radiation that is incident on a cloudy sky at latitude ϕ, and is calculated here from cloud amount based on monthly climatology via (Goodwin and Williams, 2023),

https://doi.org/10.5194/egusphere-2023-2307
Preprint. Discussion started: 24 October 2023

$$f_{CI}(\phi) = \frac{\sum f_{CA}(\phi,m) R_{solar}(\phi,m) \Delta t_m}{\sum R_{solar}(\phi,m) \Delta t_m} \quad (8)$$

where $f_{CA}(\phi, m)$ and $R_{solar}(\phi, m)$ are monthly- and zonal-mean values during month m, Δt_m is the one-twelfth of a year, and the summation occurs over all 12 months. Therefore, the fraction of cloud-incident solar radiation, $f_{CI}(\phi)$, accounts for monthly variations in cloudiness and solar radiation but not sub-monthly variations.

The emissivity and albedo for the climatological period July 2005 to June 2015 are reconstructed as annual- and zonal-means for clear-sky, all-sky and cloudy-sky conditions (Figures 3, 4) by applying eqs. (6) and (7) to observational and re-analysis products.

2.1 Defining climate feedback for uniform surface warming or relative to zonal warming

The annual- and zonal-mean climate feedback for cloud-state i at latitude ϕ relative to local warming, $\lambda_i^*(\phi)$ in $Wm^{-2}K^{-1}$, is defined here as minus the differential of outgoing radiation at the top-of-atmosphere under cloud state i with respect to surface temperature,

$$\lambda_i(\phi) = -\frac{\partial R_{out,i}}{\partial T_S}(\phi) = -\frac{\partial}{\partial T_S}[\varepsilon_i(\phi)\sigma T_S^4(\phi) + \alpha_i(\phi) R_{solar}(\phi)] \quad (9a)$$

where $R_{out,i}$ and T_S are both annual- and zonal-means. Noting that σ and $R_{solar}(\phi)$ are unaffected by Earth's surface temperature, eq. (9a) is expressed,

$$\lambda_i(\phi) = -\underbrace{4\varepsilon_i(\phi)\sigma T_S^3(\phi)}_{Planck} - \underbrace{\sigma T_S^4(\phi)\frac{\partial \varepsilon_i}{\partial T_S}(\phi)}_{WVLR+LWcloud} - \underbrace{R_{solar}(\phi)\frac{\partial \alpha_i}{\partial T_S}(\phi)}_{albedo+SWCloud} \quad (9b)$$

where the three terms on the right-hand side represent the Planck feedback; the water vapour-lapse rate plus longwave cloud feedbacks; and the surface albedo plus shortwave cloud feedbacks, respectively. $\lambda_i(\phi)$ represents the climate feedback relative to zonal warming, while taking the global area-weighted mean of $\lambda_i(\phi)$ provides the global area-weighted mean climate feedback for a uniform surface warming, $\overline{\lambda_{i,uniform}}$. Our aim will be to evaluate the zonal-mean $\lambda_i(\phi)$ drawing on approximate functional relationships for each climate feedback component in eq. (9b) using theory and observational constraints, excluding the cloud feedbacks.

2.2 Defining climate feedback for a specified warming pattern

Current observed surface warming is not uniform (e.g. Morice et al., 2021), and so the effective global mean climate feedback for recent warming must be calculated by weighting $\lambda_i(\phi)$ by the amount of recent warming across ϕ. We define the warming-weighted climate feedback at latitude ϕ, $\lambda_i^*(\phi)$ in $Wm^{-2}K^{-1}$, as,

$$\lambda_i^*(\phi) = -\frac{\partial R_{out,i}}{\partial T_S}(\phi)\frac{\partial T_S}{\partial \overline{T_S}}(\phi) = \lambda_i(\phi)\frac{\partial T_S}{\partial \overline{T_S}}(\phi) \quad (10)$$

where $\frac{\partial T_S}{\partial \overline{T_S}}(\phi)$ represents the warming of annual- and zonal-mean surface temperature per unit warming of annual- and global-mean surface temperature. The weighted climate feedback is evaluated here from recent observed warming (Morice et al.,

https://doi.org/10.5194/egusphere-2023-2307
Preprint. Discussion started: 24 October 2023

2021), $\frac{\partial T_S}{\partial \overline{T_S}}(\phi) \approx \frac{\delta T_S}{\delta \overline{T_S}}(\phi)$. In the observational analysis presented here, we adopt the recent warming for the period 2005-2015 relative to the 1961-1990 average (Fig. 5, black) to calculate $\lambda_i^*(\phi)$, since the goal is to calculate climate feedback from climatological data and theory. There are other reasonable choices, for example the projected equilibrium warming patterns following a 4xCO_2 experiment in climate models (Fig. 5, orange) and these alternative choices are reserved for future study since the goal here is to evaluate climate feedbacks from observations. The global effective climate feedback for recent warming is then the area-mean value of $\lambda_i^*(\phi)$, eq. (10c). All evaluations of climate feedback with latitude in this study (e.g. Figure 6) refer to the definitions in eqns. (9a) and (9b), as do evaluations of global mean climate feedbacks for uniform warming (Fig. 2, grey). The evaluations of global mean climate feedback for recent warming patterns use the definition in eq. (10c). Since different models and observable periods may have different warming patterns, it may be a fairer comparison of climate feedbacks to consider $\lambda_i(\phi)$ rather than $\lambda_i^*(\phi)$, since differences in the change in outgoing radiation per unit warming at some latitude may be affected by either the local climate feedback or the relative warming at that latitude, eqns (9) and (10).

2.3 Evaluating climate feedback for uniform and specified warming patterns

Since we have been free to choose the definitions for emissivity and albedo, eq. (6), relations (5)-(10) are true in the general case. However, to evaluate $\lambda_i(\phi)$ and $\lambda_i^*(\phi)$ from observational constraints the dependencies of $\frac{\partial \varepsilon_i}{\partial T_S}$ and $\frac{\partial \alpha_i}{\partial T_S}$ in eq. (9) must now be established, which requires approximations and assumptions to be made. First, we consider the non-cloud longwave feedbacks (involving Planck and water vapour-lapse rate feedbacks: Section 3) and then the shortwave non-cloud feedbacks (involving the surface albedo feedback: Section 4) assuming that climatological cloudiness with latitude remains constant in time and evaluated using annual and zonal means. The overall climate feedback from all processes is evaluated and discussed (Section 5), using previous estimated ranges for the cloud feedback.

3 Longwave non-cloud climate feedback

The Planck feedback at constant specific humidity expresses the instantaneous change in outgoing radiation due to a change in surface temperature with all atmospheric constituents held constant, including the specific humidity, lapse rate and cloud state. The water vapour-lapse rate (WVLR) feedback then expresses the change in outgoing radiation following the water vapour and lapse rate responses to surface warming, with cloud state held constant. By contrast, the temperature feedback at constant relative humidity (Held and Shell, 2012) expresses the change in outgoing radiation due to a change in surface temperature where the specific humidity and lapse rate are allowed to respond such that relative humidity is held constant. Sections 3.1 and 3.2 consider the Planck, WVLR and temperature feedbacks under clear skies. Section 3.3 then considers the impact of clouds on emissivity to evaluate the Planck, WVLR and temperature feedbacks under cloudy-sky and all-sky conditions. In this section, longwave feedbacks are calculated assuming climatological cloudiness with latitude remains constant in time.

https://doi.org/10.5194/egusphere-2023-2307
Preprint. Discussion started: 24 October 2023

3.1 Planck feedback (constant specific humidity) under clear skies

The Planck feedback at constant specific humidity is the longwave climate feedback component for constant atmospheric composition, such that emissivity remains constant. Under clear sky conditions, the Planck feedback at constant specific humidity is given, from eq. 9, by,

$$\lambda_{Planck:specific,ClearSky}(\phi) = -4\varepsilon_{ClearSky}(\phi)\sigma T_S^3(\phi) \quad (11)$$

Taking the recent observational climatology values for $\varepsilon_{ClearSky}(\phi)$ (Fig. 3b) and T_S^3 (where temperature is raised to the third power prior to zonal and annual averaging), $\lambda_{Planck:specific,ClearSky}(\phi)$ is evaluated (Fig. 6a, red), revealing a global mean value of $\overline{\lambda_{Planck:specific,ClearSky}} = -3.71$ Wm^{-2}K^{-1}.

3.2 Clear sky longwave feedbacks

The aim here is to explore the Water Vapour Lapse Rate (WVLR) feedback under clear-sky conditions, which from eq. (9) is written,

$$\lambda_{WVLR,ClearSky}(\phi) = -\sigma T_S^4(\phi)\frac{\partial \varepsilon_{ClearSky}}{\partial T_S}(\phi) \quad (12)$$

To evaluate $\lambda_{WVLR,ClearSky}(\phi)$, the value of $\frac{\partial \varepsilon_{ClearSky}}{\partial T_S}(\phi)$ is evaluated, first by constructing an approximate functional form relationship and then using observed zonal-climatology to constrain the relationship's parameter values. We postulate that annual- and zonal mean clear sky emissivity may be approximated using a function of annual- and zonal-mean values of surface temperature, T_s, surface relative humidity, H_{rel}, and the height of the tropopause, z_{trop},

$$\varepsilon_{ClearSky} \approx f(T_s, H_{rel}, z_{trop}) \quad (13)$$

since all three parameters, T_s, H_{rel} and z_{trop}, are related to the water vapour content from the surface to the top of the atmosphere, and emissivity is strongly related to water vapour content as a greenhouse gas.

From theory and data, we find an approximate relationship for annual- and zonal-mean $\frac{\partial \varepsilon_{ClearSky}}{\partial T_S}$ in terms of T_S (Appendix B; Figure 7; eq. 12) of,

$$\frac{\partial \varepsilon_{ClearSky}}{\partial T_S} \approx -(242.96 \pm 10.01)/T_S^2 \quad (14)$$

This approximation, eq. (14), holds when local $\left|\frac{\partial z_{trop}}{\partial T_S}\right|$ is significantly less than ~1 km K^{-1} and local $\left|\frac{\partial H_{rel}}{\partial T_S}\right|$ is significantly less than ~2.5 % K^{-1}. For example, if local annual- and zonal-mean surface temperatures are warmed by 2 K, then we may use eq. (14) to calculate $\frac{\partial \varepsilon_{ClearSky}}{\partial T_S}$ provided annual- and zonal-mean tropospheric height has changed by significantly less than 2 km and annual- and zonal-mean surface relative humidity has changed by significantly less than 5 %. Here, we calculate climate feedbacks assuming that approximation (14) holds; evaluating the impacts of the full relation (Appendix B) is reserved for future study.

https://doi.org/10.5194/egusphere-2023-2307
Preprint. Discussion started: 24 October 2023

3.2.1 Clear sky WVLR feedback zonally and for uniform surface warming

Using equations (14) and (12), $\lambda_{WVLR,ClearSky}(\phi)$ is evaluated with latitude from recent climatology (Fig. 6c, red), giving a global mean of $\overline{\lambda_{WVLR,ClearSky}} = 1.14 \pm 0.05$ Wm^{-2}K^{-1} for uniform surface warming, eq. (9).

The clear-sky temperature feedback at constant relative humidity expresses the outgoing radiation response to surface temperature after water vapour and lapse rate responses act to restore relative humidity values. From eq. (9) the clear sky temperature feedback at constant relative humidity is given by,

$$\lambda_{T:relative,ClearSky}(\phi) = -4\varepsilon_{ClearSky}(\phi)\sigma T_S^3(\phi) - \sigma T_S^4(\phi)\frac{\partial \varepsilon_{ClearSky}}{\partial T_S}(\phi) \quad (15)$$

and is evaluated with latitude from recent climatology (Fig. 6b, red), including using eq. (14) for $\frac{\partial \varepsilon_{ClearSky}}{\partial T_S}$, giving a global mean estimate of $\overline{\lambda_{T:relative,ClearSky}} = -2.56 \pm 0.05$ Wm^{-2}K^{-1} for uniform surface warming.

3.2.2 Clear sky WVLR feedback for recent warming

When modulated by the recent observed warming pattern, eq. (10c), the clear-sky global mean WVLR feedback and temperature feedback at constant relative humidity are only slightly altered to become $\overline{\lambda^*_{WVLR,ClearSky}} = 1.13 \pm 0.05$ Wm^{-2}K^{-1} and $\overline{\lambda^*_{T:relative,ClearSky}} = -2.53 \pm 0.05$ Wm^{-2}K^{-1} respectively.

3.3 Cloud impact on longwave feedbacks

The impacts of clouds on emissivity and the Planck and WVLR feedbacks are now assessed, with annual- and zonal-mean cloud amount assumed to remain constant in response to changes in surface temperature, $\frac{\partial f_{CA}}{\partial T_S} = 0$. Terms with non-zero $\frac{\partial f_{CA}}{\partial T_S}$ will contribute to a separate cloud feedback, which is reserved for future study.

3.3.1 Longwave feedbacks zonally and for uniform surface warming

The Planck feedback at constant specific humidity under cloudy sky conditions is obtained from eq. (9), via

$$\lambda_{Planck:specific,CloudySky}(\phi) = -4\varepsilon_{CloudySky}(\phi)\sigma T_S^3(\phi) \quad (16)$$

where $\varepsilon_{CloudySky}$ (Fig. 3b, blue) represents the annual- and zonal-mean cloudy-sky emissivity averaged over all cloud types present at that latitude. $\lambda_{Planck:specific,CloudySky}(\phi)$ is evaluated with latitude from recent climatology (Fig. 6a, blue), giving a global mean value $\overline{\lambda_{Planck:specific,CloudySky}} = -3.08$ Wm^{-2}K^{-1} (Table 1). Similarly, the Planck feedback at constant specific humidity under all-sky conditions becomes, from eq. (9),

$$\lambda_{Planck:specific,AllSky}(\phi) = -4\varepsilon_{AllSky}(\phi)\sigma T_S^3(\phi) \quad (17)$$

https://doi.org/10.5194/egusphere-2023-2307
Preprint. Discussion started: 24 October 2023

and is evaluated with latitude from recent climatology, (Fig. 6a, black) and the global mean value is assessed (Fig. 2a, grey; Table 1), with $\overline{\lambda_{Planck:specific,AllSky}} = -3.32$ Wm^{-2}K^{-1} for uniform surface warming. The value of $\lambda_{Planck:specific,AllSky}$ assessed here (Figs. 2,6; Table 1) is consistent with pre-existing estimates (e.g. IPCC, 2021; Sherwood et al., 2020; Zelinka et al., 2020).

The next goal is to evaluate the WVLR feedback under cloudy sky and all sky conditions, where from eq. (9),

$$\lambda_{WVLR,CloudySky}(\phi) = -\sigma T_S^4(\phi)\frac{\partial \varepsilon_{CloudySky}}{\partial T_S}(\phi) \quad (18)$$

and

$$\lambda_{WVLR,AllSky}(\phi) = -\sigma T_S^4(\phi)\frac{\partial \varepsilon_{AllSky}}{\partial T_S}\Big|_{\delta f_{CA}=0}(\phi) \quad (19)$$

where $\frac{\partial \varepsilon_{AllSky}}{\partial T_S}$ is evaluated at constant cloud amount, $\delta f_{CA} = 0$. For this, approximate relationships are required expressing how the presence of clouds affect the sensitivity of emissivity to surface temperature under cloudy sky and all sky conditions; $\frac{\partial \varepsilon_{CloudySky}}{\partial T_S}$ and $\frac{\partial \varepsilon_{AllSky}}{\partial T_S}$ relative to $\frac{\partial \varepsilon_{ClearSky}}{\partial T_S}$.

Appendix C explores the impact on annual- and zonal-mean bulk emissivity and cloud amount fraction via an empirically motivated cloud-emissivity coefficient, defined (Goodwin and Williams, 2023) as,

$$c_\varepsilon(\phi) = \frac{[1-\varepsilon_{CloudySky}(\phi)]}{[1-\varepsilon_{ClearSky}(\phi)]} \quad (20)$$

which is found here to take a near-uniform value of $c_\varepsilon = 1.37 \pm 0.06$ over all latitudes for the period June 2005 to July 2015 (Fig. 3d; Appendix C). The near uniform value of c_ε with latitude (Fig. 3d), where T_S varies by order 70 K (Figs. 1, 7a), implies that c_ε will not change significantly in response to altered surface temperatures, and this is exploited in developing our closures for longwave climate feedbacks (Appendix C). Noting that $\frac{\partial \varepsilon_{CloudySky}}{\partial T_S} = c_\varepsilon \frac{\partial \varepsilon_{ClearSky}}{\partial T_S}$ from the near constancy of $c_\varepsilon(\phi)$ in eq. (20), and combining this with eq. (18), the water vapour-lapse rate feedback under cloudy sky conditions becomes,

$$\lambda_{WVLR,CloudySky}(\phi) = -c_\varepsilon\, \sigma T_S^4(\phi)\frac{\partial \varepsilon_{ClearSky}}{\partial T_S}(\phi) \quad (21)$$

Using a uniform $c_\varepsilon = 1.37 \pm 0.06$ for all latitudes (Fig. 3d; Appendix C), $\lambda_{WVLR,CloudySky}(\phi)$ is evaluated from recent climatology (Fig. 6c, blue), resulting in a global area-weighted mean cloudy-sky water vapour-lapse rate feedback of $\overline{\lambda_{WVLR,CloudySky}} = -1.57 \pm 0.09$ Wm^{-2}K^{-1} for uniform surface warming.

The temperature feedback at constant relative humidity in cloudy-sky conditions is expressed by combining eq. (21) and (16),

$$\lambda_{Temp:relative,CloudySky}(\phi) = -4\varepsilon_{CloudySky}(\phi)\sigma T_S^3(\phi) - c_\varepsilon\, \sigma T_S^4(\phi)\frac{\partial \varepsilon_{ClearSky}}{\partial T_S}(\phi) \quad (22)$$

https://doi.org/10.5194/egusphere-2023-2307
Preprint. Discussion started: 24 October 2023

and is evaluated from recent climatology (Fig. 6b, blue), revealing a global mean cloudy-sky temperature feedback at constant relative humidity of $\overline{\lambda_{T:relative,CloudySky}} = -1.50 \pm 0.09$ Wm^{-2}K^{-1} for uniform surface warming.

Substituting the definition of c_ε (eq. 24) into eq. (7a) and differentiating with respect to surface temperature at constant cloud amount, $\delta f_{CA} = 0$, and assuming constant c_ε under temperature change, $\frac{\partial c_\varepsilon}{\partial T_S} \approx 0$, reveals the relation between the sensitivity of all-sky emissivity to surface temperature and the sensitivity of clear-sky emissivity to surface temperature,

$$\left.\frac{\partial \varepsilon_{AllSky}}{\partial T_S}\right|_{\delta f_{CA}=0}(\phi) = f_{CA}(\phi)\frac{\partial \varepsilon_{CloudySky}}{\partial T_S}(\phi) + [1 - f_{CA}(\phi)]\frac{\partial \varepsilon_{ClearSky}}{\partial T_S}(\phi) \quad (23)$$

Substituting in c_ε to remove the $\frac{\partial \varepsilon_{CloudySky}}{\partial T_S}(\phi)$ term gives,

$$\left.\frac{\partial \varepsilon_{AllSky}}{\partial T_S}\right|_{\delta f_{CA}=0}(\phi) = [1 - f_{CA}(\phi) + f_{CA}(\phi)c_\varepsilon]\frac{\partial \varepsilon_{ClearSky}}{\partial T_S}(\phi) \quad (24)$$

The WVLR feedback under all sky conditions is obtained by substituting eq. (24) into eq. (19) giving,

$$\lambda_{WVLR,AllSky}(\phi) = -\sigma T_S^4[1 - f_{CA} + f_{CA}c_\varepsilon]\frac{\partial \varepsilon_{ClearSky}}{\partial T_S}(\phi) \quad (25)$$

which is evaluated latitudinally (Fig. 6c, black) and as global mean, $\overline{\lambda_{WVLR,AllSky}} = 1.41 \pm 0.07$ Wm^{-2}K^{-1} for uniform surface warming (Table 1; Fig. 2c, grey), consistent with previous estimates and complex Earth system models (e.g. IPCC, 2021; Sherwood et al., 2020; Zelinka et al., 2020).

The temperature feedback at constant relative humidity (e.g. Held and Shell, 2012; Zelinka et al., 2020), under all-sky conditions is then given by substituting eq. (24) into eq. (9) giving,

$$\lambda_{T:relative,AllSky}(\phi) = -4\varepsilon_{AllSky}(\phi)\sigma T_S^3(\phi) - \sigma T_S^4(\phi)\left.\frac{\partial \varepsilon_{AllSky}}{\partial T_S}\right|_{\delta f_{CA}=0}(\phi) \quad (26)$$

which when expressed in terms of $\frac{\partial \varepsilon_{ClearSky}}{\partial T_S}$ using (25) becomes,

$$\lambda_{T:relative,AllSky} = -4\varepsilon_{AllSky}\sigma T_S^3 - \sigma T_S^4[1 - f_{CA} + f_{CA}c_\varepsilon]\frac{\partial \varepsilon_{ClearSky}}{\partial T_S}(\phi) \quad (27)$$

Evaluating from recent climatology reveals the latitudinal pattern (Fig. 6c, black) with global mean value $\overline{\lambda_{T:relative,AllSky}} = -1.92 \pm 0.07$ (Table 1 for median and percentile ranges; Fig. 2b, grey) for uniform surface warming.

3.3.2 Longwave feedbacks for recent surface warming

When modulated by the recent observed warming pattern, eq. (10c), the cloudy sky longwave feedbacks become: $\overline{\lambda^*_{Planck:specific,CloudySky}} = 3.06$ Wm^{-2}K^{-1} for the Planck feedback; $\overline{\lambda^*_{WVLR,CloudySky}} = -1.55 \pm 0.09$ Wm^{-2}K^{-1} for the WVLR feedback; and $\overline{\lambda^*_{T:relative,CloudySky}} = -1.51 \pm 0.09$ Wm^{-2}K^{-1} for the temperature feedback at constant relative humidity. The

https://doi.org/10.5194/egusphere-2023-2307
Preprint. Discussion started: 24 October 2023

all sky longwave feedbacks for recent surface warming become: $\overline{\lambda^*_{Planck:specific,AllSky}} = -3.30$ Wm^{-2}K^{-1} for the Planck feedback (Fig. 2a, black; Table 1); $\overline{\lambda^*_{WVLR,AllSky}} = 1.38 \pm 0.07$ Wm^{-2}K^{-1} for the WVLR feedback (Fig. 2c, black; Table 1); and $\overline{\lambda^*_{T:relative,AllSky}} = -1.92 \pm 0.07$ for the temperature feedback at constant relative humidity (Fig. 2b, black; Table 1).

375

3.3.3 Discussion of longwave feedback estimates

The estimates of $\lambda_{Planck:relative,AllSky}$ and $\lambda_{WVLR,AllSky}$ produced here (Fig. 2b,c; Fig. 6b,c; Table 1) are obtained from approximate functional relationships constrained by recent climatology, and make the following assumptions:

- $c_\varepsilon = 1.37 \pm 0.07$ for all latitudes, and $\frac{\partial c_\varepsilon}{\partial T_S} = 0$; such that there is no change in cloud emissivity coefficient with
380 surface temperature, supported by figure 3d showing c_ε is near-uniform with latitude.
- $\varepsilon_{ClearSky} \approx A + B \ln H_{rel} + C z_{trop} + \frac{D}{T_S}$; as supported by figure 7c, agreement between red and black lines.
- $\frac{\partial z_{trop}}{\partial T_S} \approx 0$ and $\frac{\partial H_{rel}}{\partial T_S} \approx 0$; or, more precisely the terms are less than the direct temperature term when differentiating eq. 17: $\left|C \frac{\partial z_{trop}}{\partial T_S}\right| \ll \left|\frac{D}{T_S^2}\right|$ and $\left|\frac{B}{H_{rel}} \frac{\partial H_{rel}}{\partial T_S}\right| \ll \left|\frac{D}{T_S^2}\right|$, implying that $\frac{\partial z_{trop}}{\partial T_S} \ll 1$ km K^{-1} and $\frac{\partial H_{rel}}{\partial T_S} \ll 2$ % K^{-1}.

385 These assumptions are independent from the assumptions made by previous methodologies (e.g. Sherwood et al., 2020; IPCC, 2021; Zelinka et al., 2020), while the estimates produced here are in good agreement with these previous studies (Table 1; Figure 2), providing independent evidence for the evaluated climate feedback values.

The estimates of temperature feedback at constant relative humidity, both for uniform surface warming and recent surface
390 warming, are in excellent agreement with the complex Earth system models analysed by Zelinka et al. (2020) (Table 1; Fig. 2b, compare black and grey to red and orange). Note that while the Zelinka et al. (2020) analysis calculates the slightly different Planck feedback at constant relative humidity (Held and Shell, 2012), which does not include lapse rate adjustment, the values are expected to be similar to those presented here (eq. 31) since the mean adjustment from the lapse rate feedback at constant relative humidity in the CMIP6 models is only -0.05 Wm^{-2}K^{-1} (Zelinka et al., 2020; see Supplementary Information therein).

395

4 Shortwave non-cloud climate feedback

Shortwave radiation interacts with the Earth's surface, with clouds and with atmospheric water vapour, such that the overall shortwave climate feedback arises from combined responses of surface, water vapour and cloud properties to warming. This section considers the shortwave non-cloud feedback from changes in Earth's surface properties and atmospheric water vapor
400 content. The impact of clouds is considered separately below (Section 5). The method presented is designed around the surface

https://doi.org/10.5194/egusphere-2023-2307
Preprint. Discussion started: 24 October 2023

albedo feedback, as this is larger than the shortwave water vapour feedback (e.g. Sherwood et al., 2020). However, it should be noted that formally the smaller shortwave water vapour shortwave feedback is implicitly included within the observational constraints used to determine the albedo feedback through the empirical design, but the closures fitted to the observational constraints only functionally consider the surface albedo processes. The surface albedo feedback depends crucially on the temperature-dependence of surface albedo with latitude. Annual- and zonal-mean surface albedo in clear-sky conditions varies significantly with latitude in recent climatology, with high values at the high-latitude polar regions (indicating greater reflection of incident solar radiation) and lower values at the low latitude regions (indicating less reflection) (Fig. 8a, red). Plotting in temperature space (Fig. 8b), the colder regions have higher surface albedo, while the warmer regions have lower surface albedo.

There are many factors that affect the annual- and zonal-mean surface albedo, including: the annual- and zonal-mean extent of the cryosphere; the fraction of the land and ocean at that latitude, where ocean generally has a smaller albedo and land; the vegetation-type on land; the latitude itself affecting the incidence angle of incoming solar radiation, where large angles of incidence at higher latitudes may be expected to lead to a greater fraction of reflected radiation.

The observed variation in surface clear-sky albedo (Figs. 8a,b, red) reflects all contributing factors. The largest increases in albedo occur from ~±60° latitude to the poles (Fig. 8a, red), coinciding with increasing extent of the cryosphere as annual- and zonal-mean surface temperatures fall below ~280 K (Fig. 8b). The goal here is to extract the impact of surface temperature on surface albedo via the cryosphere, $\frac{\partial \alpha_{ClearSky}}{\partial T_S}$, from all the other factors affecting the observed data (Fig. 8a,b) such as via changing land vegetation-type for temperatures above when the cryosphere acts. In this section, shortwave feedbacks are calculated assuming climatological cloudiness with latitude remains constant in time.

4.1 Clear sky shortwave feedback

From eq. (9) the clear-sky surface albedo feedback is expressed,

$$\lambda_{albedo,ClearSky}(\phi) = -R_{solar}(\phi)\frac{\partial \alpha_{ClearSky}}{\partial T_S}(\phi) \quad (28)$$

The aim now is to calculate change in clear sky (surface) albedo with temperature, $\frac{\partial \alpha_{ClearSky}}{\partial T_S}$, due to temperature-dependent changes in the extent of the cryosphere. First, we assume that the annual- and zonal-mean clear-sky albedo at latitude ϕ is a function of both surface temperature (due to the cryosphere changing the reflectivity of the surface) and latitude (due to the solar zenith angle changing the reflectivity of the surface), $\alpha_{ClearSky} \approx f(T_S, \phi)$. Therefore, the sensitivity of clear-sky albedo to surface temperature is also a function of both temperature and latitude, $\frac{\partial \alpha_{ClearSky}}{\partial T_S} \approx f(T_S, \phi)$. We must now select some functional form relating $\alpha_{ClearSky}$ and $\frac{\partial \alpha_{ClearSky}}{\partial T_S}$ to T_S and ϕ.

https://doi.org/10.5194/egusphere-2023-2307
Preprint. Discussion started: 24 October 2023

An approximate functional form relating the sensitivity of clear-sky annual- and zonal-mean albedo to surface temperature at temperature T_S and latitude ϕ is set out in Appendix D,

$$\frac{\partial \alpha_{ClearSky}}{\partial T_S}(\phi, T_S) = \left[1 + \left[\frac{1}{2}[3\sin^2\phi - 1]\right]\right]\frac{\partial \overline{\alpha_{ClearSky}}}{\partial T_S}(T_S) \quad (29)$$

where: ; $\overline{\alpha_{ClearSky}}(T_S)$ represents the global mean clear-sky albedo if the entire Earth's surface fixed at temperature T_S, and is assumed to take a cubic functional form between two temperature limits, corresponding to the temperature at which seasonal snow starts to settle and the temperature at which the entire surface is ice covered, and be constant outside those limits (Fig. 8c, grey line, and see Goodwin and Williams, 2023).

4.1.1 Clear sky shortwave feedback zonally and for uniform surface warming

Substituting this approximation, eq. (29), into eq. (28) reveals the clear-sky surface albedo feedback with latitude, $\lambda_{albedo,ClearSky}(\phi)$ (Fig. 6d, red), and produces a global mean value, $\overline{\lambda_{albedo,ClearSky}} = 0.47 \pm 0.07$ Wm^{-2}K^{-1} for uniform surface warming; where independent Gaussian uncertainties in T_{cold} and T_{warm} of ±0.5K, and in $\overline{\alpha_{cold}}$ and $\overline{\alpha_{warm}}$ of ±0.01, are applied. This clear sky albedo feedback for uniform surface warming is consistent with a set of 15 CMIP6 models, who have a multi-model mean of 0.49 Wm^{-2}K^{-1} following an abrupt 4xCO_2 forcing (Appendix A; Figure 6d, orange), with a range from 0.39 to 0.60 Wm^{-2}K^{-1}.

4.1.2 Clear sky shortwave feedback for recent surface warming

Since the largest warming occurs at high northern latitudes corresponding to areas with high zonal climate feedback (Fig. 7, Fig. 6d), the clear sky albedo feedback is significantly increased to $\overline{\lambda^*_{albedo,ClearSky}} = 0.75 \pm 0.07$ Wm^{-2}K^{-1} under the recent warming pattern, relative to the global mean feedback under uniform surface warming (0.47 ± 0.07 Wm^{-2}K^{-1}).

4.2 Cloud impact on shortwave non-cloud feedback

The goal is to evaluate the cloudy-sky and all-sky surface albedo feedbacks in the presence of clouds, but assuming that clouds do not respond to surface temperature change, $\frac{\partial f_{CI}}{\partial T_S} = 0$. The impact on albedo of cloud response to surface warming, $\frac{\partial f_{CI}}{\partial T_S} \neq 0$, is reserved for future study. Differentiating eq. (7b) with respect to surface temperature at constant cloud incident radiation fraction, $\frac{\partial f_{CI}}{\partial T_S} = 0$, we have,

$$\frac{\partial \alpha_{AllSky}}{\partial T_S} = f_{CI}\frac{\partial \alpha_{CloudySky}}{\partial T_S} + [1 - f_{CI}]\frac{\partial \alpha_{ClearSky}}{\partial T_S} \quad (30)$$

The goal is to evaluate how the presence of clouds alters the albedo contribution to shortwave feedback in cloudy sky $\frac{\partial \alpha_{CloudySky}}{\partial T_S}$ relative to clear sky $\frac{\partial \alpha_{ClearSky}}{\partial T_S}$, eq. (30).

https://doi.org/10.5194/egusphere-2023-2307
Preprint. Discussion started: 24 October 2023

4.2.1 All sky and cloudy sky shortwave feedback zonally and for uniform surface warming

Appendix E finds an approximate relation between the albedo of cloud (if all light that passed through the cloud were absorbed) and the albedo of a cloudy sky (eq. E3), obtained by considering an infinite series approach after Taylor et al. (2007), extended here to explicitly include separate diffuse and directed shortwave beams (Figure 9). The implied albedo of cloud is then evaluated from data (Fig. 8a, black; Appendix E) and a relation is identified between $\frac{\partial \alpha_{CloudySky}}{\partial T_S}$ and $\frac{\partial \alpha_{ClearSky}}{\partial T_S}$,

$$\frac{\partial \alpha_{CloudySky}}{\partial T_S} = \left[\frac{[1-\alpha_{Cloud:dir}(\phi)][1-\overline{\alpha_{Cloud}}]}{[1-\overline{\alpha_{ClearSky}}(\phi)\overline{\alpha_{Cloud}}]^2\left[1+\left[0.5\times[3\sin^2\phi-1]\right]\right]}\right]\frac{\partial \alpha_{ClearSky}}{\partial T_S} \quad (31)$$

where $\alpha_{Cloud:dir}(\phi)$ is the albedo of cloud for directed solar radiation at latitude ϕ (Figure 9); $\overline{\alpha_{Cloud}}$ is the global mean albedo of cloud at all latitudes (assumed equal to the albedo of cloud for diffuse shortwave light, $\alpha_{Cloud:diff}$ in Figure 9); and $\overline{\alpha_{ClearSky}}(\phi)$ is the planetary albedo for directed incident solar radiation if the entire Earth's surface were the same as the surface at latitude ϕ (assumed equal to the clear sky albedo for diffuse shortwave light at latitude ϕ, $\alpha_{surface:diff}$ in Figure 9).

The surface albedo feedback for cloudy sky conditions is then obtained from eqs. (9) and (31), giving,

$$\lambda_{albedo,CloudySky}(\phi) = -R_{solar}(\phi)\frac{[1-\overline{\alpha_{Cloud}}][1-\alpha_{Cloud:dir}(\phi)]}{[1-\overline{\alpha_{ClearSky}}\,\overline{\alpha_{Cloud}}]^2\left[1+\left[0.5\times[3\sin^2\phi-1]\right]\right]}\frac{\partial \alpha_{ClearSky}}{\partial T_S} \quad (32)$$

Evaluating this surface albedo feedback from recent climatology reveals the zonal climate feedback with latitude (Fig. 6d, blue) with a global mean value of $\overline{\lambda_{albedo,CloudySky}} = 0.11 \pm 0.02$ Wm^{-2}K^{-1} for uniform surface warming.

The overall surface albedo feedback under all sky conditions with constant cloudiness is then obtained from eqs. (7), (9), (30) and (31), giving,

$$\lambda_{albedo,AllSky}(\phi) = -R_{solar}(\phi)\left[f_{CI}\frac{[1-\overline{\alpha_{Cloud}}][1-\alpha_{Cloud:dir}]}{[1-\overline{\alpha_{ClearSky}}\,\overline{\alpha_{Cloud}}]^2\left[1+\left[0.5\times[3\sin^2\phi-1]\right]\right]}+[1-f_{CI}]\right]\frac{\partial \alpha_{ClearSky}}{\partial T_S} \quad (33)$$

Evaluating the surface albedo feedback from recent climatology reveals the latitudinal pattern (Fig. 6d, black and grey; Table 1), while the mean and standard deviation of the area-weighted global mean surface albedo feedback are, $\overline{\lambda_{albedo,AllSky}} = 0.21 \pm 0.03$ Wm^{-2}K^{-1} for uniform surface warming. This all-sky albedo feedback for uniform surface warming is smaller than previous estimates of albedo feedback (Table 1, Fig. 2, compare grey to blue, orange and red), and this may reflect how polar amplification of surface warming enhances the contribution of melting snow and ice at high latitudes towards the global energy balance.

4.2.1 All sky and cloudy sky shortwave feedback for recent surface warming

https://doi.org/10.5194/egusphere-2023-2307
Preprint. Discussion started: 24 October 2023

When modulated by recent surface warming (Fig. 7; eq. 10) the global mean cloudy sky albedo feedback increases to $\overline{\lambda^*_{albedo,CloudySky}} = 0.18 \pm 0.02$ Wm^{-2}K^{-1}, while the all sky albedo feedback (Fig. 2d, compare black to grey) increases to $\overline{\lambda^*_{albedo,AllSky}} = 0.37 \pm 0.04$ Wm^{-2}K^{-1}. This global mean value for recent surface warming is consistent with previous analyses of the surface albedo feedback (IPCC, 2021; Sherwood et al., 2020; Zelinka et al., 2020; Fig. 2d, compare black to blue, orange and red), confirming that the method presented here (eqs. 28-33; figs. 8,9) is consistent with previous surface albedo estimates when the enhancement of snow and ice melt on global energy balance through polar amplification of warming (eq. 10; fig. 5), is accounted for. Note that here the shortwave water vapour feedback is included within the overall surface albedo feedback.

4.3 Discussion of albedo feedback

The latitudinal pattern shows peaks in each hemisphere ~±65° latitude, corresponding to regions where changing temperatures most alter the extent of the cryosphere, along with a hemispheric asymmetry at higher latitudes where larger $\lambda_{albedo,AllSky}$ values extending towards the poles in the Northern hemisphere but $\lambda_{albedo,AllSky}$ decreasing towards zero in the southern hemisphere (Fig. 6d, black). These latitudinal traits (Fig. 6d, black) are consistent with the numerical models analysed by Zelinka and Hartmann (2012: see Fig. 3 therein) and Colman and Hanson (2017: see Fig. 4 therein), and 15 CMIP6 models with zonal climate feedback analysed using radiative kernels (Fig. 6d, compare black to orange; Appendix E), demonstrating that the approximate functional relationship (33) suitably captures latitudinal properties emerging in mechanistic analyses.

The estimates of λ_{albedo} produced here (Fig. 2b,c; Fig. 6b,c; Table 1) are obtained from approximate functional relationships constrained by recent climatology, and make the following assumptions:

- There is no change in cloud albedo with surface temperature, $\frac{\partial \alpha_{Cloud:dir}}{\partial T_S} = 0$, supported by figure 4d showing that $\alpha_{\mathrm{Cloud:dir}}$ is primarily a function of latitude due to zenith angle effect.
- Incident solar radiation is directed, whereas reflected shortwave and emitted longwave radiation is diffuse.
- The annual- and zonal-mean albedo for directed solar radiation incident on a particular surface is dependent on latitude, via a second-order Legendre polynomial in sine of latitude (Appendix D, eq. D3; Fig. 8a).
- The global mean albedo over all latitudes for directed solar radiation incident on an entire planet covered in a particular surface j is equal to the albedo for diffuse radiation incident on that surface at any latitude, $\overline{\alpha_{j:dir}} = \alpha_{j:diff}(\phi)$ for all ϕ. These two assumptions are both supported by figs. 4d, 9d, where cloud is the surface type and the relation is approximately a 2nd order Legendre polynomial.
- The global mean clear-sky albedo for a surface cooler than 5 °C and warmer than some colder temperature at which the surface is entirely dominated by the cryosphere is approximated by a cubic in $T_S$with turning points at 5°C and the colder temperature, supported by figure 8c, compare grey line to red dots.

These assumptions are independent from the assumptions used in previous studies, calculated using time-varying properties in models and/or observations (e.g. Zelinka et al., 2020; Sherwood et al., 2020; IPCC, 2021; Zelinka and Hartmann, 2012;

https://doi.org/10.5194/egusphere-2023-2307
Preprint. Discussion started: 24 October 2023

Colman and Hanson, 2017), while the estimates are in good agreement with these previous studies (e.g. Fig. 2; Table 1), supporting the use of the approximate functional relationships presented here (eqs. 9, 10, 30 to 33).

5 Total net climate feedback

The total climate feedback with latitude is found by combining the Planck (specific), WVLR, surface albedo and cloud feedbacks via,

$$\lambda_{total,AllSky}(\phi) = \lambda_{Planck:specific,AllSky}(\phi) + \lambda_{WVLR,AllSky}(\phi) + \lambda_{albedo,AllSky}(\phi) + \lambda_{Cloud,AllSky}(\phi) \quad (34)$$

or equivalently use the temperature feedback at constant relative humidity using, $\lambda_{total,AllSky}(\phi) = \lambda_{T:relative,AllSly}(\phi) + \lambda_{albedo,AllSky}(\phi) + \lambda_{Cloud,AllSky}(\phi)$. Since no estimate of cloud feedback is produced here, the global mean total net climate feedback is estimated by combining the global estimates of Planck, WVLR and albedo feedback with a recent estimate of global cloud feedback from multiple lines of evidence: 0.45 ± 0.33 $Wm^{-2}K^{-1}$ (Sherwood et al., 2020).

5.1 Total net climate feedback zonally and for uniform surface warming

Combining eqs. (17), (25), (33) with a global net cloud feedback of 0.45 ± 0.33 $Wm^{-2}K^{-1}$ (Sherwood et al., 2020), the net climate feedback under all-sky conditions is evaluated from recent climatology with latitude, $\lambda_{total,AllSky}(\phi)$ (Fig. 6e) giving a global area-weighted mean $\overline{\lambda_{total,AllSky}} = -1.25 \pm 0.34$ $Wm^{-2}K^{-1}$ (Table 1) for uniform surface warming. The magnitude and uncertainty in total net climate feedback, $\overline{\lambda_{total,AllSky}}$, is consistent with previous estimates using different methodologies (IPCC, 2021; Sherwood et al., 2020; Zelinka et al., 2019).

5.2 Total net climate feedback for recent surface warming

The net climate feedback modulated by the recent warming pattern, comprising the sum of $\overline{\lambda^*_{Planck,AllSky}}$, $\overline{\lambda^*_{WVLR,AllSky}}$, $\overline{\lambda^*_{albedo,AllSky}}$, and the Sherwood et al. (2020) estimate for cloud feedback (eq. 34), produces a global mean of $\overline{\lambda^*_{total,AllSky}} = -1.10 \pm 0.34$ $Wm^{-2}K^{-1}$ (Fig. 2e, black; Table 1). This global mean climate feedback for patterned warming is also consistent with previous estimates (Fig. 2f, Table 1), including the IPCC AR6 best estimate of $= -1.16$ $Wm^{-2}K^{-1}$.

6 Climate feedback discussion

This study has presented a novel method to evaluate climate feedback by exploiting variations in climate properties over latitude (such as surface temperature) in order to predict the radiative response to an external forcing (Figs. 2; 6 Table 1; eqs. 5-34). This method is independent from, but complementary to, the existing methods where variation in climate properties over time is used to evaluate climate feedback (e.g. Sherwood et al., 2020; IPCC, 2020).

6.1 Net climate feedback estimates from latitudinal variation in outgoing radiation and surface temperature

https://doi.org/10.5194/egusphere-2023-2307
Preprint. Discussion started: 24 October 2023

Three estimates of total net global climate feedback from latitudinal variation in outgoing radiation and surface temperature are presented in this study. Firstly, a regression of climatological annual- and zonal-mean values of outgoing radiation and surface temperature at 5° latitude resolution (Fig. 1) produces a global mean $\lambda_{total} \approx -\delta[L_{out} + S_{out}]/\delta T_S = -1.30 \pm 0.06$ $Wm^{-2}K^{-1}$, and assumes that $\delta[L_{out} + S_{out}]/\delta T_S = \partial[L_{out} + S_{out}]/\partial T_S$. However, while 93% of the variance in outgoing radiation with latitude is linked to variance in surface temperature with latitude in the regression (Fig. 1), this estimate ignores how some portion of outgoing radiation variance may be linked to other properties that co-vary latitudinally with temperature in the climatological mean, but do not co-vary similarly with temperature *change* following perturbation.

The second estimate then uses theory to solve for $\lambda = -\partial[L_{out} + S_{out}]/\partial T_S$ directly (eqns. 9-34), thus extracting only the portion of variance with latitude of outgoing radiation that is directly due to changes temperature. Performing a simple area mean gives $\overline{\lambda_{total,AllSky}} = -1.25 \pm 0.34$ $Wm^{-2}K^{-1}$ (Fig. 2e, grey; Table 1). The relative change in best estimates (-1.30 to -1.25 $Wm^{-2}K^{-1}$) implies that factors other than temperature act to increase the equator to pole difference in outgoing radiation by order 7 Wm^{-2}. Factors that affect outgoing radiation and co-vary with surface temperature in the climatological mean include: the balance between the decrease in incident solar radiation with latitude (Fig. 4a) and the increase in albedo of a uniform surface-type with latitude (Fig. 8a) modulating outgoing shortwave radiation via $S_{out}(\phi) = \alpha(\phi)R_{solar}(\phi)$; and decrease in the height of the tropopause with latitude (Fig. 7c) modulating outgoing longwave radiation (Table 2, negative value for coefficient C). This second estimate, of $\overline{\lambda_{total,AllSky}} = -1.25 \pm 0.34$ $Wm^{-2}K^{-1}$, ignores how areas with greater surface warming will make a greater contribution to the global mean climate feedback.

The third estimate presented here both solves for $\lambda = -\partial[L_{out} + S_{out}]/\partial T_S$ directly (eqns. 9-34) and accounts for how areas with greater surface warming make a greater contribution to global mean climate feedback (eq. 10), giving $\overline{\lambda^*_{total,AllSky}} = -1.10 \pm 0.34$ $Wm^{-2}K^{-1}$ (Fig. 2e, black; Table 1). The more positive climate feedback value for this third warming-weighted estimate, $= -1.10 \pm 0.34$ $Wm^{-2}K^{-1}$, relative to the unweighted area-mean, -1.25 ± 0.34 $Wm^{-2}K^{-1}$ (Fig. 2e, compare black to grey; Table 1) reflects how areas with greatest warming at high northern latitudes (Fig. 5) have more positive (amplifying) local climate feedbacks (Fig. 6h), thus contributing to a more positive global mean climate feedback.

6.2 Comparison of results to previous studies

Here, separate climate feedback terms are evaluated for Planck feedback (constant specific humidity), water vapour-lapse rate feedback, temperature feedback (constant relative humidity) and surface albedo feedback. The global area-weighted mean climate feedbacks for all terms are in good agreement with other previous methodologies (Table 1; Fig. 2), including evaluation from complex Earth system models (e.g. Zelinka et al., 2020), and evaluation from multiple lines of evidence (e.g. IPCC, 2020; Sherwood et al., 2020). The agreement for albedo feedback is significantly improved when the zonal climate feedback is

https://doi.org/10.5194/egusphere-2023-2307
Preprint. Discussion started: 24 October 2023

weighted by the recent warming (Fig. 2, black; eq. 10) compared to when the a uniform surface warming is assumed (Fig. 2, grey).

The spatial patterns of feedbacks (Fig. 6) are also in good agreement with the multi-model mean climate feedback following an abrupt 4xCO_2 perturbation experiment in 15-CMIP6 models, evaluated using radiative kernels (Fig. 6a, c, d, and e: compare black to orange; Appendix A). The spatial pattern of the surface albedo feedback is also similar to other numerical model evaluations (Fig. 6, compare to Colman and Hanson, 2017 and Zelinka and Hartmann, 2012; Figure 6e, compare to e.g. Sherwood et al., 2020). Note that for the 4xCO_2 perturbation experiment the overall climate change is significant, while the evaluation from recent climatology is for infinitesimal perturbation.

The agreement, in terms of both the global mean values and the spatial patterns (Fig. 2, Fig. 6), indicates that our approximate functional relationships (eqs. 5-34) are adequately capturing the system to allow climate feedbacks to be constrained from the observed latitudinal variation in recent climatology.

6.3 Comparison of methodology to previous studies

Previous methods include constraining climate feedbacks from perturbed numerical model experiments (e.g. Soden et al., 2008; Zelinka et al., 2020); from observations of temporal changes in observed climate in response to forcing (e.g. Otto et al., 2013; Goodwin and Cael, 2020; Cael et al., 2023); from observed short-timescale variability in the climate state (Dessler, 2013); and applying emergent constraints to complex climate models (e.g. Cox et al., 2018). This study's approach is independent of many these previous methodologies: firstly, being based on latitudinal variation not temporal variation and, secondly, being based on differentiated infinitesimal perturbation rather than finite perturbation, resulting in a different set of assumptions.

Mauritsen et al. (2013) showed that individual climate feedbacks acting separately do not simply linearly add to produce the overall climate feedback when all process act together in a complex climate model under finite perturbation. However, when separating individual climate feedbacks from numerical model experiments using finite CO_2 perturbation experiments (e.g. Soden et al., 2008; Zelinka et al., 2020) a required assumption is that the total climate feedback is composed to individual climate feedbacks are linearly separable (compare eqn. 4 to eqn. 1). Crucially, as the functional relationships we employ are explicitly differentiated to find climate feedback, we do not need to assume that climate feedbacks are linearly separable (as is required when separating climate feedback terms from numerical model experiments using finite CO_2 perturbation experiments: e.g. Soden et al., 2008; Zelinka et al., 2020). For the CMIP6 models analysed in Zelinka et al. (2020), the value of the sum of the individual feedbacks, $\sum_X \lambda_X$, ranges from 0.37 $Wm^{-2}K^{-1}$ larger to -0.25 $Wm^{-2}K^{-1}$ smaller than the net feedback λ. It is possible that this overall error when assuming $\lambda \approx \sum_X \lambda_X$ (eq. 3) arises because of a combination of offsetting errors

https://doi.org/10.5194/egusphere-2023-2307
Preprint. Discussion started: 24 October 2023

affecting the individual feedbacks, some of which could be larger in magnitude than the overall error. The approach presented here does not need to make the linearly separable assumption (eq. 3), and so this possible source of error does not apply.

The method presented here does not need to quantify temporal changes either in radiative forcing or Earth's energy balance, both of which carry significant uncertainty (which is required when evaluating climate feedback from temporal historical observations: e.g. Otto et al., 2013; Goodwin and Cael, 2020). For example, there is high uncertainty in historic radiative forcing due to uncertainty in the radiative impact of changing aerosol levels.

6.4 Implications for climate sensitivity and future work

The equilibrium climate sensitivity (ECS in K) is approximately related to the global average climate feedback via $ECS \approx F_{2xCO2}/\overline{\lambda^*}$, where F_{2xCO2} is the radiative forcing for doubling of CO_2. Using of F_{2xCO2}~3.8 Wm^{-2} (Sherwood et al., 2020; using stratospherically adjusted radiative forcing definition), the overall net climate feedback evaluated here for the recent warming pattern (Fig. 2, black; Table 1: $\overline{\lambda^*} = -1.10$ (-0.76 to -1.44) $Wm^{-2}K^{-1}$) is broadly consistent with an equilibrium climate sensitivity of ~3.5 K warming for a doubling of CO_2, ranging from 2.6 to 5.0 K.

Other estimates based on recent observations, that consider temporal changes often provide a current climate feedback close to $\overline{\lambda^*} \sim -2$ $Wm^{-2}K^{-1}$ during the anthropogenic warming over recent decades, consistent with an ECS of 2K (e.g. Otto et al., 2013; and, specifically for the instantaneous time evolving climate feedback in the very recent past, Cael et al., 2023 and Goodwin, 2021). Our result of $\overline{\lambda^*} \sim -1$ $Wm^{-2}K^{-1}$ differs since, by considering latitudinal variation in recent observations, we estimate the *equilibrium* climate feedback for non-cloud feedback combined with an independent estimate of net cloud feedback (Sherwood et al., 2020) and, correspondingly, we acquire a value closer to previous estimations at equilibrium (e.g. Sherwood et al., 2020; IPCC, 2021; Table 1).

We anticipate that analysis of numerical Earth system model output using the functional forms presented here will also prove a useful avenue of research. Ultimately, it may be possible to evaluate the climate feedbacks in complex numerical models using latitudinal variation in outgoing radiation, surface temperatures and cloud amount, provided the numerical model output is consistent with how the observations are obtained: e.g. simulated cloud amount must represent what would be *optically* measured from satellites (Karlsson et al., 2021), and not calculated based on the *thermodynamics* of the simulated cloud coverage. The latitudinal variation method for calculating climate feedback presented here can also be extended to include alternative approximate functional relationships, differing to those presented used in this study, eqs. (11)-(34); Appendices B, C, D, E.

https://doi.org/10.5194/egusphere-2023-2307
Preprint. Discussion started: 24 October 2023

Appendix A: Kernel decomposition of zonal climate feedbacks in 15 CMIP6 models

Climate feedbacks for uniform surface warming in 15 CMIP6 models is calculated using a radiative kernel decomposition (of radiation changes following an abrupt 4xCO_2 forcing experiment. The climate feedbacks considered are calculated as a time-average using the final 20-years of a 150-year experiment. The following equation is used,

$$\lambda_X(\phi) = -\frac{\delta R_X}{\delta T_S}(\phi) \quad \text{(A1)}$$

where both R_X and T_S are annual- and zonal-averages. The values of $\lambda_X(\phi)$ are plotted in Figure 6 (orange dotted lines) for the Planck, albedo and WVLR feedbacks. The 15 CMIP6 models included are: BCC-C2SM2-MR, BCC-ESM1, CESM2-WACCM, CESM2, CNRM-CM6_1, CNRM-ESM2-1, GFDL_CM4, GISS-E2-1-G, GISS-E2-1-H, HadGEM3-GC31-LL, IPSL-CM6A-LR, MIROC6, MRI-ESM2-0, SAM0-UNICON, and UKESM1-0-LL.

Appendix B: Observational constraints on clear sky emissivity relation to surface temperature

To postulate an approximate functional relationship for eq. (13), three assumptions are made:

(1) emissivity decreases with the natural logarithm of the total vertically integrated water vapour content of the atmosphere, m_{WV},

$$\Delta\varepsilon_{ClearSky} \approx A\Delta \ln m_{WV} \quad \text{(B1)}$$

where A is a coefficient whose value relates to this equation only;

(2) the total vertically integrated water vapour content in the atmosphere is a function of surface specific humidity and the height of the tropopause at that location,

$$m_{WV} \approx AH_{specific} \exp\left(Bz_{trop}\right) \quad \text{(B2)}$$

where atmospheric density is assumed to reduce exponentially with height, where A and B are coefficients whose values relate to this equation only; and

(3) the functional form of the Clausius-Clapeyron relation explains the link between relative humidity and specific humidity,

$$H_{specific} \approx AH_{rel} \exp\left(B + \frac{C}{T_S}\right) \quad \text{(B3)}$$

where A, B and C are coefficients whose values relate to this equation only;

These three assumptions, eqs. (B1), (B2) and (B3), combine to produce a functional approximation of the form,

$$\varepsilon_{ClearSky} \approx A + B \ln\left(H_{rel} \exp\left(Cz_{trop}\right) \exp\left(D + \frac{E}{T_S}\right)\right) \quad \text{(B4)}$$

where A, B, C, D, E and F are coefficients. This simplifies to a relation of the form,

$$\varepsilon_{ClearSky} \approx A + B \ln H_{rel} + Cz_{trop} + \frac{D}{T_S} \quad \text{(B6)}$$

where the values of coefficients A, B, C and D are not preserved. Applying a regression to observational annual-and zonal-mean climatological values for H_{rel} (Hersbach et al., 2018: ERA5), z_{trop} (Mateus et al., 2022: bilinear interpolation model

https://doi.org/10.5194/egusphere-2023-2307
Preprint. Discussion started: 24 October 2023

therein and for a surface at 3.0 potential vorticity units, where 1 potential vorticity unit is equal to 10^{-6} K kg^{-1} m^2 s^{-1}), T_S (Jones et al., 1999; Morice et al., 2021: CRUTEM and HadCRUT5) and $\varepsilon_{ClearSky}$ (Fig. 3b) we find values of the coefficients A, B, C and D such that variation H_{rel}, z_{trop} and T_S explain 98.8% of the variance in $\varepsilon_{ClearSky}$ across latitudes in the climatological mean, based on the adjusted R-squared value (Fig. 7; Table 2). Given the goodness of fit, the postulated relationship, eq. (B6), is accepted in this study. Exploring alternative approximate functional forms is reserved for future study.

The sensitivity of clear-sky emissivity to surface temperature is calculated from differentiating eq. (B6) with respect to surface temperature, giving,

$$\frac{\partial \varepsilon_{ClearSky}}{\partial T_S} = \frac{B}{H_{rel}}\frac{\partial H_{rel}}{\partial T_S} + C\frac{\partial z_{trop}}{\partial T_S} - \frac{D}{T_S^2} \quad \text{(B7)}$$

which approximates, under the assumption that tropospheric height and surface relative humidity do not significantly change with surface warming, $\left|\frac{\partial z_{trop}}{\partial T_S}\right| \ll \left|\frac{D}{CT_S^2}\right|$ and $\left|\frac{\partial H_{rel}}{\partial T_S}\right| \ll \left|\frac{H_{rel}}{B}\frac{D}{T_S^2}\right|$, to,

$$\frac{\partial \varepsilon_{ClearSky}}{\partial T_S} \approx -\frac{D}{T_S^2} \approx -(242.96 \pm 10.01)/T_S^2 \quad \text{(B8)}$$

Inspecting the values of the coefficients A, B, C and D (Table 2), and typical values of H_{rel} and T_S, this approximation (B8) holds when local $\left|\frac{\partial z_{trop}}{\partial T_S}\right|$ is significantly less than ~1 km K^{-1} and local $\left|\frac{\partial H_{rel}}{\partial T_S}\right|$ is significantly less than ~2.5 % K^{-1}. For example, if local annual- and zonal-mean surface temperatures are warmed by 2 K, then we may use (B8) to calculate $\frac{\partial \varepsilon_{ClearSky}}{\partial T_S}$ provided annual- and zonal-mean tropospheric height has changed by significantly less than 2 km and annual- and zonal-mean surface relative humidity has changed by significantly less than 5 %. Here, we calculate climate feedbacks assuming that approximation (B8) holds; evaluating the impacts of the full relation (B7) is reserved for future study.

Appendix C: Impact of clouds on bulk emissivity

To consider how the emissivity is affected by clouds, first consider the difference between cloudy-sky emissivity and clear-sky emissivity with latitude (Fig. 3b, blue and orange). A perfect black body with no atmosphere has a bulk emissivity of 1. The introduction of a clear sky Earth-like atmosphere reduces the bulk emissivity, $\varepsilon_{ClearSky} < 1$, principally through water vapour which absorbs longwave radiation. The introduction of clouds within the atmosphere then reduces the bulk emissivity further, $\varepsilon_{CloudySky} < \varepsilon_{ClearSky} < 1$, because clouds too absorb longwave radiation. The question is: how does the presence of cloud affect bulk emissivity, $\varepsilon_{CloudySky}$, relative to a clear-sky atmosphere, $\varepsilon_{ClearSky}$, and relative to a black body with no atmosphere, 1.

https://doi.org/10.5194/egusphere-2023-2307
Preprint. Discussion started: 24 October 2023

Goodwin and Williams (2023) found empirically find that the value of $\varepsilon_{CloudySky} - \varepsilon_{ClearSky}$ (or equivalently the value of $1 - \varepsilon_{CloudySky}$) scales with the value of $1 - \varepsilon_{ClearSky}$, so that $\varepsilon_{ClearSky} - \varepsilon_{CloudySky}$ is largest when $\varepsilon_{ClearSky}$ is smallest, and $\varepsilon_{ClearSky} - \varepsilon_{CloudySky}$ is smallest when $\varepsilon_{ClearSky}$ is largest. This finding is repeated here, updated by evaluating all terms during the July 2005 to June 2015 period (Fig. 3b, blue and orange).

The ratio of $1 - \varepsilon_{CloudySky}(\phi)$ to $1 - \varepsilon_{ClearSky}(\phi)$ for July 2005 to June 2015 is consistently ~ 1.37 across all latitudes (Fig. 3d), expressed here by adopting a dimensionless cloud-emissivity coefficient, c_ε, defined as,

$$c_\varepsilon(\phi) = \frac{[1-\varepsilon_{CloudySky}(\phi)]}{[1-\varepsilon_{ClearSky}(\phi)]} \quad \text{(C1)}$$

Evaluating the cloud-emissivity coefficient for recent climatology reveals a near-uniform value with latitude (Fig. 2d), even though surface temperatures alter by order 70 K with latitude, with an area-weighted mean and area-weighted standard deviation of $c_\varepsilon = 1.37 \pm 0.06$. Note that this updates the numerical value obtained by Goodwin and Williams (2023) of 1.38±0.10, as here all variables are evaluated for the same 10-year climatological period. This near uniformity with latitude suggests that the value of c_ε is insensitive to changes in surface temperature, $\frac{\partial c_\varepsilon}{\partial T_S} \approx 0$. Given the near-uniform value of c_ε with latitude (eq. 24; Fig. 3d), the model of consistent amplification of emissivity reduction per unit cloud amount is accepted.

What physical interpretations could explain this approximation with consistent c_ε with latitude (eq. C1; Fig. 3d)? One possibility is that latitudes with greater water vapour content in the air-column both have a greater reduction in clear-sky bulk emissivity (relative to 1), and also have cloud types, cloud altitudes and cloud-induced lapse rate adjustments that cause a greater reduction in bulk emissivity (eq. 6). Conversely, latitudes with lesser water vapour content in the air-column have both the lesser reduction in emissivity in clear-sky conditions (relative to 1) and form cloud-types, cloud altitudes and cloud-adjustments to the lapse rate that cause lesser reduction in bulk emissivity (eq. 6). In other words, clear sky emissivity reduction, and the emissivity reduction from clouds formed, both scale similarly with the water vapour content of the air-column. An alternative possibility is that emissivity reduction from water vapour and emissivity reduction from clouds combine geometrically, rather than arithmetically, in determining the total emissivity reduction (relative to 1) in an air column with both water vapour and clouds.

Appendix D: Clear-sky surface albedo as a function of latitude and temperature

A function utilising a second-order Legendre polynomial in the sine of latitude approximates the variation in annual- and zonal-mean incoming solar radiation per unit surface area with latitude to within a few percent at all latitudes (e.g. Hartmann, 1994),

https://doi.org/10.5194/egusphere-2023-2307
Preprint. Discussion started: 24 October 2023

$$R_{solar}(\phi) \approx \overline{R_{solar}}\left[1 - p\left[\frac{1}{2}[3\sin^2\phi - 1]\right]\right] \quad \text{(D1)}$$

where $\overline{R_{solar}}$ is the annual- and global-mean solar radiation per unit surface area given by $\overline{R_{solar}} = \frac{\int R_{solar}(\phi)dA}{\int dA}$, and $p \approx 0.477$ is a tuned coefficient. This relation for $R_{solar}(\phi)$, eq. (28), approximates the inverse of the average surface area over which solar radiation is incident upon with latitude, given that the solar zenith angle varies both with time of day and seasonally and the length of the day varies seasonally. Note the minus sign before the coefficient p, which exists because $R_{solar}(\phi)$ is greatest at low latitudes and least at high latitudes.

The aim here is to postulate a similar relation that will describe how annual- and zonal-mean local albedo, $\alpha(\phi)$, varies with latitude, given that the albedo for a particular surface-type will vary with solar zenith angle, and solar zenith angle varies daily and seasonally, and the length of the day varies seasonally. First, consider the annual- and global-mean albedo, $\overline{\alpha_j}$, that would be achieved if the entire surface of the planet were covered with a single material j, and with no cloud above that material,

$$\overline{\alpha_j} = \frac{\int \alpha_j(\phi)dA}{\int dA} \quad \text{(D2)}$$

where $\alpha_j(\phi)$ is the local annual- and zonal-mean albedo at latitude ϕ for material j. We now postulate that for some material j the annual- and zonal-mean albedo at latitude ϕ, $\alpha_j(\phi)$, is approximately related to the global planetary albedo for a planet covered in that material, $\overline{\alpha_j}$, through a similar functional form to the approximation for $R_{solar}(\phi)$, eq. (D1),

$$\alpha_j(\phi) = \overline{\alpha_j}\left[1 + \left[1 - \overline{\alpha_j}\right]\left[\frac{1}{2}[3\sin^2\phi - 1]\right]\right] \quad \text{(D3)}$$

Note that (1) the sign before the coefficient changes, from negative in eq. (D1) to positive in eq. (D3); and (2) that the tuned coefficient p in the incident radiation relation, eq. (D1), becomes a function of the global mean albedo for material j, $\left[1 - \overline{\alpha_j}\right]$, in the postulated albedo relation, eq. (D3). The reason the sign changes is because while $R_{solar}(\phi)$ is largest at low latitudes and smallest at high latitudes, we expect the opposite for albedo for a given material: we expect materials to become more reflective at noon at high latitudes as the annual-average solar zenith angle increases.

The reasons we postulate a coefficient that varies with $\overline{\alpha_j}$, via $\left[1 - \overline{\alpha_j}\right]$, are twofold. Firstly, it simplifies the relation by specifying local annual- and zonal-mean albedo at latitude ϕ for a given material, $\alpha_j(\phi)$, from a single property of that material: $\overline{\alpha_j}$ (eq. D3; Fig. 8a, grey). Secondly, it ensures that the equation asymptotes to sensible limits for both perfectly absorbing and perfectly reflecting surface-types (eq. D3; Fig. 8a, grey): when a planet covered in a surface-type is perfectly absorbing, $\overline{\alpha_j} = 0$, then local albedo is perfectly absorbing at all latitudes, $\alpha_j(\phi) = 0$ for all ϕ; whereas when a planet covered in a surface-type is perfectly reflecting, $\overline{\alpha_j} = 1$, then local albedo is perfectly reflecting at all latitudes, $\alpha_j(\phi) = 1$ for all ϕ. For materials with all intermediate physically plausible global albedo values, $0 < \overline{\alpha_j} < 1$, the values of $\alpha_j(\phi)$ are always physically plausible for all latitudes: $0 < \alpha(\phi) < 1$ for all ϕ (eq. D3; Fig. 8a, grey).

https://doi.org/10.5194/egusphere-2023-2307
Preprint. Discussion started: 24 October 2023

The parameter $\overline{\alpha_{ClearSky}}(\phi)$ is now defined as the annual- and global-mean clear-sky albedo for a planet covered entirely in the balance of surface-materials found at latitude ϕ. The goal is to assess how $\overline{\alpha_{ClearSky}}$ will change with surface temperature, due to changes in the cryosphere (but ignoring other surface changes that may have temperature dependence such as land-vegetation type). By considering how temperature is related to cryosphere coverage, two regions where $\frac{\partial \overline{\alpha_{ClearSky}}}{\partial T_S}(\phi) \to 0$ are identified: (1) when $T_S(\phi)$ is below some cold temperature, T_{cold}, such that the cryosphere is unchanged by further cooling, because the entire surface is ice-covered and more ice cannot be produced; and (2) when $T_S(\phi)$ is above some warm temperature, T_{warm}, such that the cryosphere is unchanged by further warming, because there is insignificant seasonal snow cover and so snow cover cannot be reduced further.

Inspecting the observed $\alpha_{ClearSky}(\phi)$ with T_S (Fig. 8b), and noting that snow and ice generally indicates a surface temperatures are near or below freezing, we assume that $\frac{\partial \overline{\alpha_{ClearSky}}}{\partial T_S} \to 0$ for $T_S > 5$°C (such that $T_{warm} = 278.15$ K), being an annual- and zonal-mean temperature below which significant parts of the year may be below freezing and so significant snow or ice may begin to affect the annual-mean albedo. It is not clear by inspecting the data for $\alpha_{ClearSky}(\phi)$ with T_S where the cold temperature, T_{cold}, should be placed, since $\alpha_{ClearSky}(\phi)$ is expected to increase with both cooler temperatures and higher latitudes, and these variables co-vary.

From the observed values of $\alpha_{ClearSky}(\phi)$ (Fig. 8a, red), the implied values of $\overline{\alpha_{ClearSky}}$ are calculated using eq. (D2) for all $T_S(\phi) < 5$ °C (Fig. 8c, red). Graphically, these $\overline{\alpha_{ClearSky}}$ values represent the intersection of grey contours and red lines in Fig. 8a. A functional form approximating $\overline{\alpha_{ClearSky}} = f(T_S)$ is now sought for $T_{cold} < T_S < T_{warm}$ (Fig. 8c), where $\frac{\partial \overline{\alpha_{ClearSky}}}{\partial T_S} \neq 0$. A cubic approximation for $\overline{\alpha_{ClearSky}}$ in T_S is chosen between temperature limits $T_{cold} < T_S < T_{warm}$, with turning points at $T_S = T_{cold}$ and $T_S = T_{warm}$, noting that the gradient of the cubic will naturally produce $\frac{\partial \overline{\alpha_{ClearSky}}}{\partial T_S} \to 0$ as $T_S \to T_{cold}$ or $T_S \to T_{warm}$, and so the values of both $\overline{\alpha_{ClearSky}}$ and $\frac{\partial \overline{\alpha_{ClearSky}}}{\partial T_S}$ will be continuous in T_S for all T_S (Fig. 8c, grey). To define the cubic approximation, four values must be specified: T_{cold}, T_{warm}, $\overline{\alpha_{cold}}$ and $\overline{\alpha_{warm}}$, where $\overline{\alpha_{cold}}$ and $\overline{\alpha_{warm}}$ are the planetary clear-sky albedos when the cryosphere entirely dominates the surface of earth ($T_S = T_{cold}$) and when the cryosphere is absent from the Earth ($T_S = T_{warm}$). The value of T_{warm} is set to 5°C (278.15 K) and then a least-squares approach is used to determine the values of T_{cold}, $\overline{\alpha_{cold}}$ and $\overline{\alpha_{warm}}$ to produce the best fit against all $\alpha_{ClearSky}(\phi)$ values when $T_S < T_{warm}$ (Fig. 8c, compare grey to red), noting that $\overline{\alpha_{ClearSky}} = \overline{\alpha_{cold}}$ when surface temperature is less than T_{cold} (Fig. 8c, grey). A minimum root-mean-square error of 0.017 albedo units is found for $T_{cold} = -31$ °C (=242.15 K); $\overline{\alpha_{cold}} = 0.43$; and $\overline{\alpha_{warm}} = 0.12$ (Fig. 8c, compare grey to red).

https://doi.org/10.5194/egusphere-2023-2307
Preprint. Discussion started: 24 October 2023

The value of $\frac{\partial \overline{\alpha_{ClearSky}}}{\partial T_S}(T_S)$ is found between $T_{cold} < T_S < T_{warm}$ by differentiating the fitted cubic for $\overline{\alpha_{ClearSky}}$ in terms of T_S (see Fig. 8c, gradient of grey dotted line), and is set to $\frac{\partial \overline{\alpha_{ClearSky}}}{\partial T_S} = 0$ outside this range. The sensitivity of annual- and zonal-mean albedo to surface temperature at temperature T_S and latitude ϕ is then found by differentiating eq. (D3),

$$\frac{\partial \alpha_{ClearSky}}{\partial T_S}(\phi, T_S) = \left[1 + \left[\frac{1}{2}[3\sin^2\phi - 1]\right]\right]\frac{\partial \overline{\alpha_{ClearSky}}}{\partial T_S}(T_S) \quad \text{(D4)}$$

Appendix E: Impact of clouds on surface albedo

Clouds act to (Fig. 9):
(1) reflect a fraction of the incident solar radiation back into space,
(2) allow some radiation to pass through; and
(3) reflect a fraction of the outgoing shortwave radiation (reflected up by the Earth's surface) back downwards towards the Earth.

Previous studies (e.g. Taylor et al., 2007) have adopted an infinite series approach to calculate the net upwards shortwave radiation above a cloudy sky given the reflections from both the clouds (in both directions) and the Earth's surface. Here, this infinite series approach is used for the global mean case, and then extended to explicitly consider separate directed and diffuse beams of shortwave radiation.

First, the annual- and global-mean albedo for cloudy sky, $\overline{\alpha_{CloudySky}}$, is expressed in terms of the annual- and global-mean albedo of cloud, $\overline{\alpha_{Cloud}}$, and the annual- and global-mean surface albedo for clear sky conditions, $\overline{\alpha_{ClearSky}}$. Note that $\overline{\alpha_{Cloud}}$ represents the fraction of incident solar radiation reflected directly by the cloud, and $\overline{\alpha_{CloudySky}}$ represents the total fraction of incident solar radiation reflected back into space above a cloudy sky – both the fraction reflected directly from the cloud and the fraction passing down through the cloud and then reflecting between the Earth's surface and the underside of the cloud until passing up through the cloud again.

Adopting an infinite series approximation to continual reflection between the Earth's surface and the underside of the cloud (e.g. Taylor et al., 2007), the annual- and global-mean albedo of cloudy sky, $\overline{\alpha_{CloudySky}}$, is expressed in terms of the annual- and global-global mean albedo of cloud itself, $\overline{\alpha_{Cloud}}$, the amount of shortwave radiation that passes through a cloud in one direction, $1 - \overline{\alpha_{Cloud}}$, and the global mean albedo of the surface in the absence of cloud, $\overline{\alpha_{ClearSky}}$, via (equivalent to eq. 7 in Taylor et al., 2007),

https://doi.org/10.5194/egusphere-2023-2307
Preprint. Discussion started: 24 October 2023

$$\overline{\alpha_{CloudySky}} \approx \overline{\alpha_{Cloud}} + \overline{\alpha_{ClearSky}} \frac{[1-\overline{\alpha_{Cloud}}]^2}{[1-\overline{\alpha_{ClearSky}} \times \overline{\alpha_{Cloud}}]} \quad \text{(E1)}$$

This expression is used to solve for $\overline{\alpha_{Cloud}}$ for the period July 2005 to June 2015, using observed climatology estimates of $\overline{\alpha_{ClearSky}}$ and $\overline{\alpha_{CloudySky}}$ (Fig. 3b), giving $\overline{\alpha_{Cloud}} = 0.30$. This observation-based estimate suggests 30% of shortwave radiation incident on a globally cloudy sky Earth would be reflected back outwards without passing through the cloud.

Next, consider the radiation that passes through the cloud. Incoming solar radiation is directed in nature. However, once shortwave radiation had reflected off a surface, or passed through cloud, it becomes largely diffuse in nature (Fig. 9, blue and red lines). Since the albedo of cloud, or Earth's surface, depends on the angle of incidence of the radiation then a distinction arises between directed solar radiation, with a single local angle of incidence that depends on the solar zenith angle, and diffuse shortwave radiation, with a range of local angle of incidences as the diffuse radiation is coming from all directions.

The distinction between angle of incidences for directed and diffuse radiation implies that the annual- and zonal-mean albedo of some surface for directed solar radiation at latitude ϕ, $\alpha_j(\phi)$, is different from the annual- and zonal-mean albedo of the same surface for diffuse radiation at latitude ϕ, $\alpha_{j:diffuse}(\phi)$. Since the global mean albedo for a planet covered in a particular surface, $\overline{\alpha_j}$ (eq. D3) reflects the effect of many angles of incidence (caused by variation in latitudes and time of day over a year), and the albedo for diffuse light also represents the effect of many angles of incidence, we make the assumption that the albedo for diffuse light for material j at latitude ϕ is approximated by the global mean albedo for a planet surface covered by the material j,

$$\alpha_{j:diffuse}(\phi) \approx \overline{\alpha_j} \quad \text{(E2)}$$

This approximation (eq. E2) allows us to make progress with extracting the local cloud albedo at different latitudes (Fig. 9).

By splitting the shortwave radiation into directed and diffuse components with distinct albedos for material j at latitude ϕ, $\alpha_j(\phi)$ and $\overline{\alpha_j}(\phi)$, the infinite series approach (e.g. Taylor et al., 2007; eq. E1) is now re-applied and extended to calculate the albedo of cloud for a directed beam with latitude, $\alpha_{Cloud:dir}(\phi)$ (Fig. 9). The annual- and zonal-mean albedo of cloudy sky at latitude ϕ, $\alpha_{CloudySky}(\phi)$, is related to the albedo of cloud for directed solar radiation at latitude ϕ, $\alpha_{Cloud}(\phi)$, the clear sky albedo for diffuse light at latitude ϕ, $\alpha_{ClearSky:diffuse}(\phi) \approx \overline{\alpha_{ClearSky}}(\phi)$ (eq. E2), and the global mean albedo of cloud, $\alpha_{Cloud:diffuse}(\phi) \approx \overline{\alpha_{Cloud}}$ (eq. E2), via

$$\alpha_{CloudySky}(\phi) \approx \alpha_{Cloud:dir}(\phi) + \overline{\alpha_{ClearSky}}(\phi) \frac{[1-\alpha_{Cloud:dir}(\phi)][1-\overline{\alpha_{Cloud}}]}{[1-\overline{\alpha_{ClearSky}}(\phi) \times \overline{\alpha_{Cloud}}]} \quad \text{(E3)}$$

Using $\alpha_{CloudySky}(\phi)$ from observations (Fig. 4b), $\overline{\alpha_{Cloud}} = 0.30$ from observational analysis of eq. (E1), and $\overline{\alpha_{ClearSky}}(\phi)$ evaluated by applying eq. (D3) to observationally constrained $\alpha_{ClearSky}(\phi)$ (Fig. 4b), the albedo of cloud with latitude is solved, $\alpha_{Cloud}(\phi)$ (Fig. 4d, Fig. 8a, black), revealing $\alpha_{Cloud}(\phi)$ values varying from around 0.19 in equatorial regions up to between 0.5 and 0.6 in polar regions.

https://doi.org/10.5194/egusphere-2023-2307
Preprint. Discussion started: 24 October 2023

Consider whether this evaluated annual- and zonal-mean α_{Cloud} profile with latitude (Figs. 4d, 7a) is reasonable. First, the evaluated magnitude of $\alpha_{Cloud}(\phi)$ and its variation with latitude (Figs. 4d, 7a) is consistent with the Stephens (1978) theoretical model and parameterisation identifying how the magnitude of cloud albedo varies with solar zenith angle (see Stephens, 1978, Figure 4 therein). Secondly, the resulting constraint on cloud albedo with latitude is in good agreement with the approximation adopted for any uniform material using a 2nd order Legendre polynomial, (eq. D3), even though this functional form is not assumed *a priori* to apply to cloud albedo in the analysis: i.e. $\alpha_{Cloud:dir}(\phi) \approx \overline{\alpha_{Cloud}}\left[1 + [1-\overline{\alpha_{Cloud}}]\left[\frac{1}{2}[3\sin^2\phi - 1]\right]\right]$, (Fig. 4d, compare black to red dashed line). Note that this functional form *is* assumed to apply to constrain $\overline{\alpha_{ClearSky}}(\phi)$ from $\alpha_{ClearSky}(\phi)$ (Fig. 8; eq. D3), when calculating $\alpha_{Cloud:dir}(\phi)$. However, the good agreement for $\alpha_{Cloud:dir}(\phi)$ (Fig. 4d, black and red) implies that, firstly, the functional form is suitable and, secondly, that the angle of incidence is a larger contributor to variation in cloud albedo than cloud-type.

Differentiating eq. (E3) with respect to surface temperature, assuming that $\alpha_{Cloud}(\phi)$ and $\overline{\alpha_{Cloud}}$ do not to vary with surface temperature, relates the sensitivity of $\alpha_{CloudySky}$ to surface temperature to the sensitivity of $\overline{\alpha_{ClearSky}}$ to surface temperature, via,

$$\frac{\partial\alpha_{CloudySky}}{\partial T_S} = \left[\frac{[1-\alpha_{Cloud:dir}(\phi)][1-\overline{\alpha_{Cloud}}]}{[1-\overline{\alpha_{ClearSky}}(\phi)\overline{\alpha_{Cloud}}]^2}\right]\frac{\partial\overline{\alpha_{ClearSky}}}{\partial T_S} \quad \text{(E4)}$$

Now substituting for $\frac{\partial\alpha_{ClearSky}}{\partial T_S}$ in terms of $\frac{\partial\overline{\alpha_{ClearSky}}}{\partial T_S}$, eq. (D4), into eq. (E4) relates cloudy sky to clear sky $\frac{\partial\alpha}{\partial T_S}$,

$$\frac{\partial\alpha_{CloudySky}}{\partial T_S} = \left[\frac{[1-\alpha_{Cloud:dir}(\phi)][1-\overline{\alpha_{Cloud}}]}{[1-\overline{\alpha_{ClearSky}}(\phi)\overline{\alpha_{Cloud}}]^2\left[1+[0.5\times[3\sin^2\phi-1]]\right]}\right]\frac{\partial\alpha_{ClearSky}}{\partial T_S} \quad \text{(E5)}$$

Code and Data Availability

CMIP data were obtained from the UK Centre for Environmental Data Analysis portal (https://esgf-index1.ceda.ac.uk/search/cmip6-ceda/). We acknowledge the WCRP, which, through its Working Group on Coupled Modeling, coordinated and promoted CMIP6. We thank the climate-modeling groups for producing and making available their model output, the Earth System Grid Federation (ESGF) for archiving the data and providing access and the multiple funding agencies that support CMIP6 and ESGF. . The CRUTEM absolute temperature record is available here (Jones et al., 1999: https://crudata.uea.ac.uk/cru/data/temperature/, downloaded 15-03-2022), and the HadCRUT5 temperature anomaly dataset is available here: version HadCRUT.5.0.1.0; Morice et al., 2021: https://www.metoffice.gov.uk/hadobs/hadcrut5/data/current/download.html, downloaded 31-10-2022. The CERES EBAF

https://doi.org/10.5194/egusphere-2023-2307
Preprint. Discussion started: 24 October 2023

Edition 4.1 satellite observational dataset for outgoing radiation is available here (Loeb et al.,2018: https://ceres.larc.nasa.gov/data/, downloaded March 14th 2022). The CLARA v2.1 dataset provides cloud amount data, available at (Karlsson et al., 2021; Copernicus Climate Change Service (C3S), 2022: accessed on 10-01-2023, https://doi.org/10.24381/cds.68653055. The climatological annual- and zonal-mean surface relative humidity, H_{rel}, we use monthly climatology for 1991 to 2000 from the European Centre for Medium Range Weather Forecasts (ECMWF) ERA5 reanalysis product, as supplied through the Copernicus Climate Change Service (C3S) through the 'Essential climate variables for assessment of climate variability from 1979 to present' (Hersbach et al., 2018: https://cds.climate.copernicus.eu/cdsapp#!/dataset/ecv-for-climate-change?tab=overview ; downloaded 31st March 2023). Code for calculating the height of the tropopause, from Mateus et al. (2022), is available for download here: https://github.com/pjmateus/global_tropopause_model (downloaded 14/04/2023); where this study uses the options for a bilinear interpolation model of the tropopause, and a surface at 3.0 potential vorticity units, where 1 potential vorticity unit is equal to 10^{-6} K kg^{-1} m^2 s^{-1}. Code for performing the analysis in this study is available at https://doi.org/10.5281/zenodo.8421164. Note that to perform the analysis the observational data must be separately downloaded from the sources above. The analysis in this study is conducted by extracting 5° latitudinal resolution data from each dataset, to match the resolution of the surface temperature datasets.

Author Contributions

PG developed the theory and conducted the numerical analysis of observational records, with input from all authors. PG led the writing of the manuscript with contributions from all authors. PC conducted the radiative kernel analysis of the 15 CMIP6 models.

Competing interests

The authors declare that they have no conflict of interest.

Acknowledgements

PG and RG acknowledge funding from UKRI NERC grant NE/T010657/1.

References

Andrews, T., Bodas-Salcedo, A., Gregory, J. M., Dong, Y., Armour, K. C., Paynter, D., Lin, P., Modak, A., Mauritsen, T., Cole, J.N.S., Medeiros, B., Benedict, J.J., Douville, H., Roehrig, R., Koshiro, T., Kawai, H., Ogura, T., Dufresne, J.-L., Allen, R.P. and Liu, C.: On the effect of historical SST patterns on radiative feedback, Journal of Geophysical Research: Atmospheres, 127, e2022JD036675, doi:10.1029/2022JD036675, 2022.

Cael, B. B., Bloch-Jonhson, J., Ceppi, P., Fredriksen, H.-B., Goodwin, P., Gregory, J.M., Smith, C.J. and Williams, R.G.: Energy budget diagnosis of changing climate feedback. *Science Advances* 9, 16, eadf9302, doi:10.1126/sciadv.adf9302, 2023.

https://doi.org/10.5194/egusphere-2023-2307
Preprint. Discussion started: 24 October 2023

Colman, R. and Hanson, L.: On the relative strength of radiative feedbacks under climate variability and change, Climate Dynamics 49, 2115-2129, doi:10.1007/s00382-016-3441-8, 2017.

Copernicus Climate Change Service (C3S): Cloud properties global gridded monthly and daily data from 1982 to present derived from satellite observations, Copernicus Climate Change Service (C3S) Climate Data Store (CDS), accessed on 10-01-2023, doi:10.24381/cds.68653055, 2022.

Cox, P., Huntingford, C. and Williamson, M.: Emergent constraint on equilibrium climate sensitivity from global temperature variability, Nature 553, 319–322, doi:10.1038/nature25450, 2018.

Dessler, A. E.: Observations of Climate Feedbacks over 2000–10 and Comparisons to Climate Models, Journal of Climate, 26, 333–342, doi:10.1175/JCLI-D-11-00640.1, 2013.

Goodwin, P.: Probabilistic projections of future warming and climate sensitivity trajectories, Oxford Open Climate Change, 1, 1, kgab007, https://doi.org/10.1093/oxfclm/kgab007, 2021.

Goodwin, P. and Cael, B.B.: Bayesian estimation of Earth's climate sensitivity and transient climate response from observational warming and heat content datasets, Earth System Dynamics, 12, 709–723, doi:10.5194/esd-12-709-2021, 2021.

Goodwin, P. and Williams, R.G.: On the Arctic Amplification of surface warming in a conceptual climate model, Physica D: Nonlinear Phenomena, doi:10.1016/j.physd.2023.133880, 2023.

Hartmann, D.L.: Global Physical Climatology, Academic Press, San Diego, USA. ISBN 0-12-328530-5. 411 pp, 1994.

Held, I.M., and Shell, K.M.: Using Relative Humidity as a State Variable in Climate Feedback Analysis, Journal of Climate 25, 2578-2582, doi:10.1175/JCLI-D-11-00721.1, 2012.

Hersbach, H., Muñoz Sabater, J., Nicolas, Rozum, I., Simmons, Vamborg, F., A., Bell, B., Berrisford, P., Biavati, G., Buontempo, C., Horányi, A., J., Peubey, C., Radu, R., Schepers, D., Soci, C., Dee, D. and Thépaut, J-N.: Essential climate variables for assessment of climate variability from 1979 to present, Copernicus Climate Change Service (C3S) Data Store (CDS), (Accessed on 31-03-2023), 2018.

Jones, P.D., New, M., Parker, D.E., Martin, S. and Rigor, I.G.: Surface air temperature and its variations over the last 150 years, Reviews of Geophysics 37, 173-199, doi:10.1029/1999RG900002, 1999.

Karlsson, K.-G., Riihelä, A., Trentmann, J., Stengel, M., Meirink, J. F., Solodovnik, I., Devasthale, A., Manninen, T., Jääskeläinen, E., Anttila, K., Kallio-Myers, V., Benas, N., Selbach, N., Stein, D., Kaiser, J., Hollmann, R.: ICDR AVHRR - based on CLARA-A2 methods, Satellite Application Facility on Climate Monitoring doi:10.5676/EUM_SAF_CM/CLARA_AVHRR/V002_01, 2021.

Loeb, N.G., Doelling, D.R., Wang, H., Su, W., Nguyen, C., Corbett, J.G., Liang, L., Mitrescu, C., Rose, F.G. and Kato, S.: Clouds and the earth's radiant energy system (CERES) energy balanced and filled (EBAF) top-of-atmosphere (TOA) edition-4.0 data product, Journal of Climate, 31(2), 895-918, doi:10.1175/JCLI-D-17-0208.1, 2018.

Mateus, P., Mendes, V.B. and Pires, C.A.L.: Global Empirical Models for Tropopause Height Determination, Remote Sensing 14, 4303, doi:10.3390/rs14174303, 2022.

https://doi.org/10.5194/egusphere-2023-2307
Preprint. Discussion started: 24 October 2023

Mauritsen, T., Graversen, R.G., Klocke, D., Langen, P.L., Stevens, B. and Tomassini, L.: Climate feedback efficiency and synergy, Climate Dynamics 41, 2539–2554, doi:10.1007/s00382-013-1808-7, 2013.

Morice, C. P., Kennedy, J. J., Rayner, N. A., Winn, J. P., Hogan, E., Killick, R. E., Dunn, R.J.H., Osborn, T.J., Jones, P.D. and Simpson, I.R.: An updated assessment of near-surface temperature change from 1850: the HadCRUT5 data set, Journal of Geophysical Research: Atmospheres, 126, e2019JD032361, doi:10.1029/2019JD032361, 2021.

Otto, A., Otto, F. E. L., Boucher, O., Church, J., Hegerl, G., Forster, P. M., Gillet, N.P., Gregory, J., Hohnson, G.C., Knutti, R., Lewis, N., Lohmann, U., Marotzke, J., Myhre, G., Shindell, D., Stevens, B. and Allen, M.R.: Energy budget constraints on climate response. Nature Geoscience, 6, 415–416, doi:10.1038/ngeo1836, 2013.

Sherwood, S. C., Webb, M. J., Annan, J. D., Armour, K. C., Forster, P. M., Hargreaves, J. C., Hegerl, G., Klein, S. A., Marvel, K. D., Rohling, E. J., Watanabe, M., Andrews, T., Braconnot, P., Bretherton, C. S., Foster, G. L., Hausfather, Z., von der Heydt, A. S., Knutti, R., Mauritsen, T., Norris, J. R., Proistosescu, C., Rugenstein, M., Schmidt, G. A., Tokarska, K. B., Zelinka, M. D. (2020). An assessment of Earth's climate sensitivity using multiple lines of evidence. Reviews of Geophysics, 58, e2019RG000678. https://doi.org/10.1029/2019RG000678

Soden, B. J., Held, I.M., Colman, R., Shell, K.M., Kiehl, J. T. and Shields, C. A.: Quantifying Climate Feedbacks Using Radiative Kernels, Journal of Climate, 21, 3504–3520, doi:10.1175/2007JCLI2110.1, 2008.

Stephens, G.L. (1978) Radiation Profiles in Extended Water Clouds. II: Parameterization Schemes. Journal of Atmospheric Sciences 35, 2123-2132, doi:10.1175/1520-0469(1978)035<2123:RPIEWC>2.0.CO;2, 1978.

Taylor, K. E., Crucifix, M., Braconnot, P., Hewitt, C. D., Doutriaux, C., Broccoli, A. J., Mitchell, J. F. B. and M. J. Webb: Estimating Shortwave Radiative Forcing and Response in Climate Models, Journal of Climate, 20, 2530–2543, doi:10.1175/JCLI4143.1, 2007.

Zelinka, M.D. and Hartmann, D.L.: Climate feedbacks and their implications for poleward energy flux changes in a warming climate, Journal of Climate 25, 608-624, doi:10.1175/JCLI-D-11-00096.1, 2012.

Zelinka, M. D., Myers, T. A., McCoy, D. T., Po-Chedley, S., Caldwell, P. M., Ceppi, P., Klein, S. A. and Taylor, K. E.: Causes of higher climate sensitivity in CMIP6 models, Geophysical Research Letters, 47, e2019GL085782, doi:10.1029/2019GL085782, 2020.

Zelinka, M. D., Zhou, C., and Klein, S. A.: Insights from a refined decomposition of cloud feedbacks, Geophys. Res. Lett., 43, 9259– 9269, doi:10.1002/2016GL069917, 2016.

https://doi.org/10.5194/egusphere-2023-2307
Preprint. Discussion started: 24 October 2023

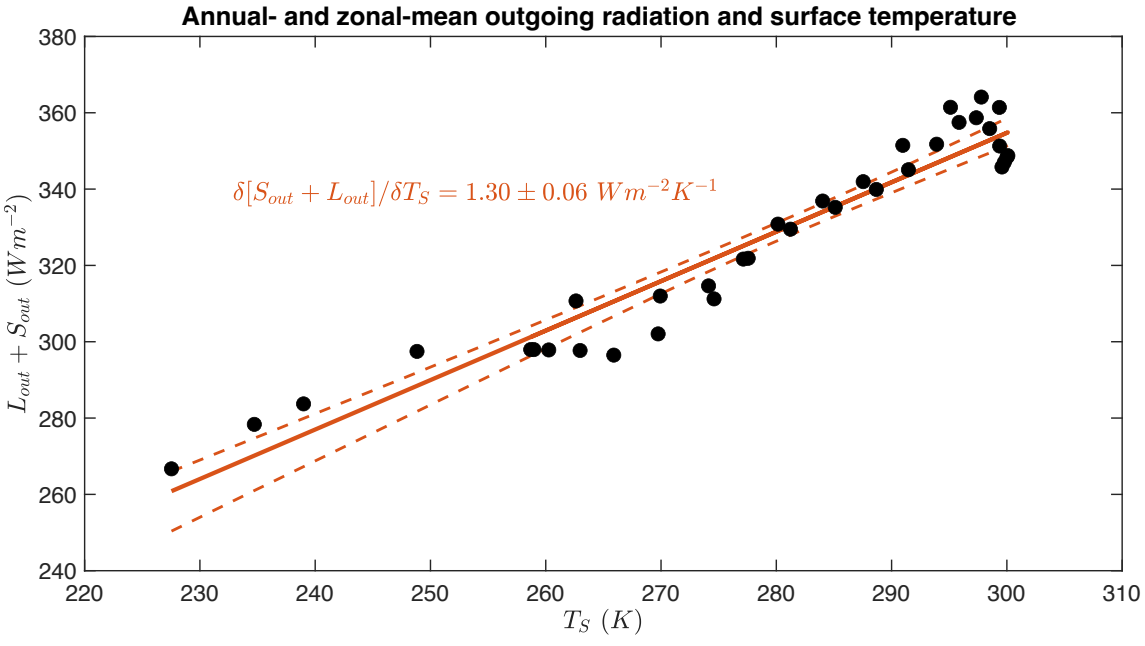

990 **Figure 1: Variation of annual- and zonal-mean shortwave plus longwave outgoing radiation at the top of the atmosphere, $S_{out} + L_{out}$, with annual- and zonal-mean surface temperature, T_S, for the period July 2005 to June 2015. Data (black) represents zonal-means spaced at 5° latitude. Also shown are the line of best fit (red solid line) and 2.5 to 97.5 % range for the line of best fit (red dashed lines).**

https://doi.org/10.5194/egusphere-2023-2307
Preprint. Discussion started: 24 October 2023

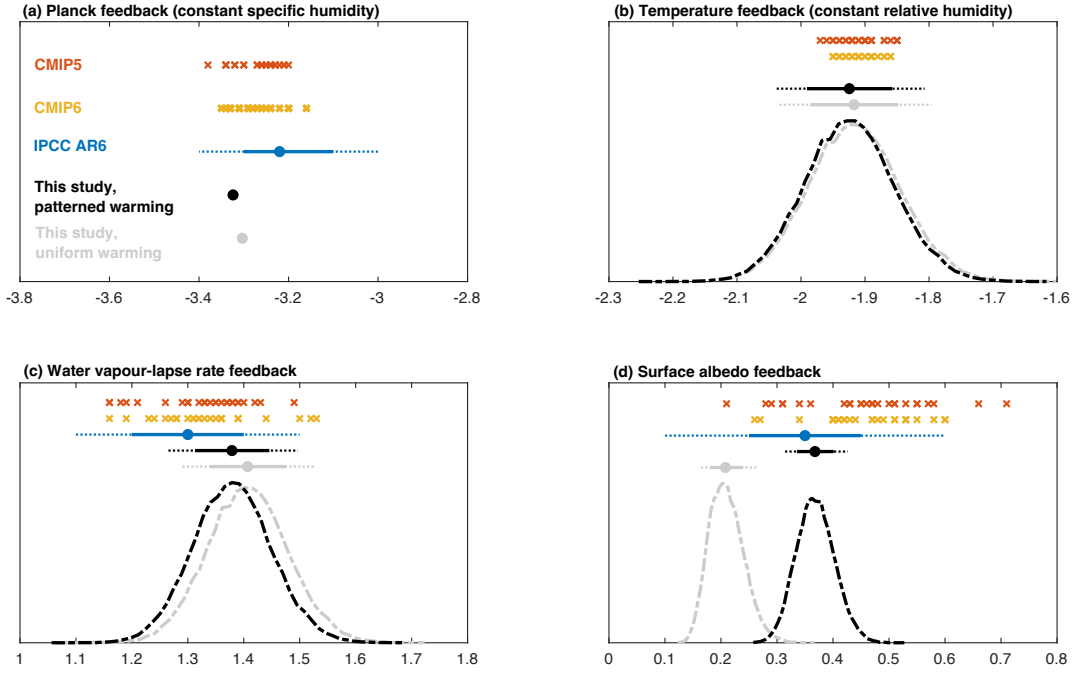

Figure 2: Global-mean climate feedback terms for (a) the Planck feedback under constant specific humidity, (b) the temperature feedback under constant relative humidity, (c) the water vapour-lapse rate feedback, (d) the surface albedo feedback. Shown are AR6 (blue: IPCC, 2021), the CMIP5 (red) and CMIP6 (orange) models (Zelinka et al., 2020) and this study (black). Dotted lines represent the 90% range, solid lines the 66% range, dots the median. The dot-dashed lines are the normalised probability density functions.

https://doi.org/10.5194/egusphere-2023-2307
Preprint. Discussion started: 24 October 2023

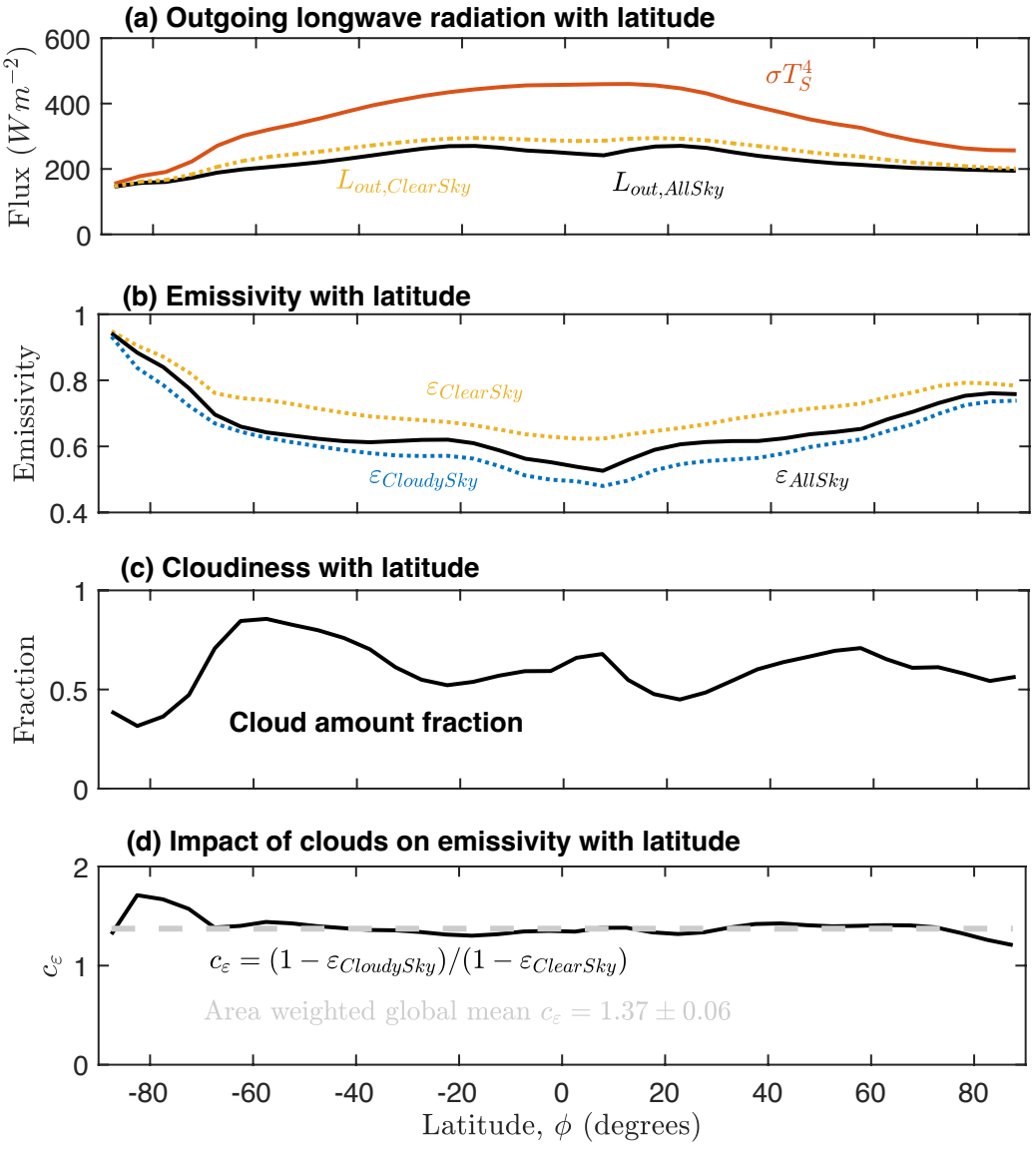

Figure 3: Longwave radiation and the impact of clouds with latitude, July 2005 to June 2015. (a) Outgoing longwave radiation at the top of the atmosphere, L_{out}, in Wm^{-2} for all sky (black line) together with clear sky (yellow dots) and the longwave dependence on surface temperature $\sigma T_S^4(\phi)$ (red line) from Loeb et al. (2018) and surface temperatures raised to the 4th power calculated from combining Jones et al. (1999) and Morice et al. (2021). (b) Emissivity values for all sky (black line), clear sky (yellow dots) and cloudy sky (blue dots) calculated from observations using eqs. (5)-(7). (c) Cloud amount from observed climatology (Karlsson et al.,2021). (d) Cloud emissivity coefficient calculated from recent climatology using eq. (20).

https://doi.org/10.5194/egusphere-2023-2307
Preprint. Discussion started: 24 October 2023

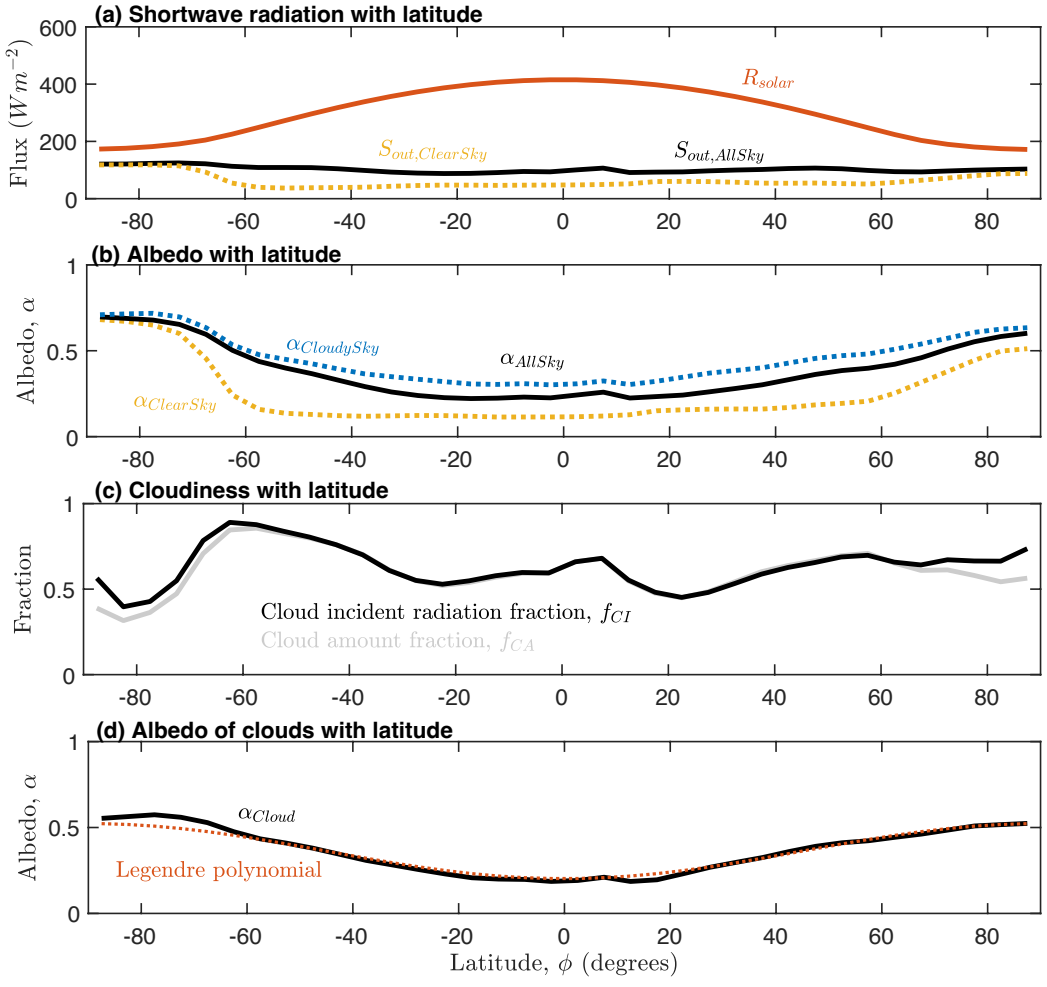

Figure 4: Shortwave radiation and the impact of clouds with latitude, July 2005 to June 2015: (a) incoming solar R_{solar} (red line) at the top of the atmosphere calculated from geometry (Hartmann, 1994) and the outgoing shortwave S_{out} for all sky (black line) in W m^{-2} at the top of the atmosphere together with estimate for cloudy sky (yellow dots) from observed climatology (Loeb et al., 2018); (b) Albedo values for all sky (black line), clear sky (yellow dots) and cloudy sky (blue dots) calculated from observed climatology and eqs. (5), (6) and (7); (c) Cloud amount from observed climatology (Karlsson et al.,2021) and cloud incident radiation fraction from observed climatology and eq. (8); (d) Albedo of clouds (black line) from recent climatology using eqs. (E1)- (E3) together with a Legendre polynomial fit (red dots).

https://doi.org/10.5194/egusphere-2023-2307
Preprint. Discussion started: 24 October 2023

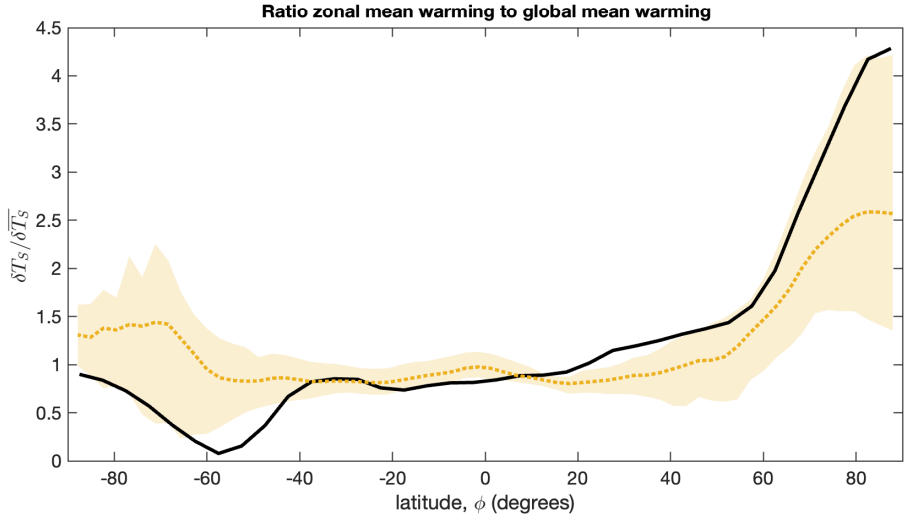

Figure 5: Recent ratio of zonal mean warming to global mean warming with latitude, $\frac{\delta T_S}{\overline{\delta T_S}}$. Analysed from HadCRUT5 (black) where recent warming is defined as the warming for the period 2005-2015 relative to 1961-1990, and for 15 CMIP6 models (orange) in years 1-20 of a 4xCO_2 forcing experiment (dotted line is multi-model mean, shaded area is range).

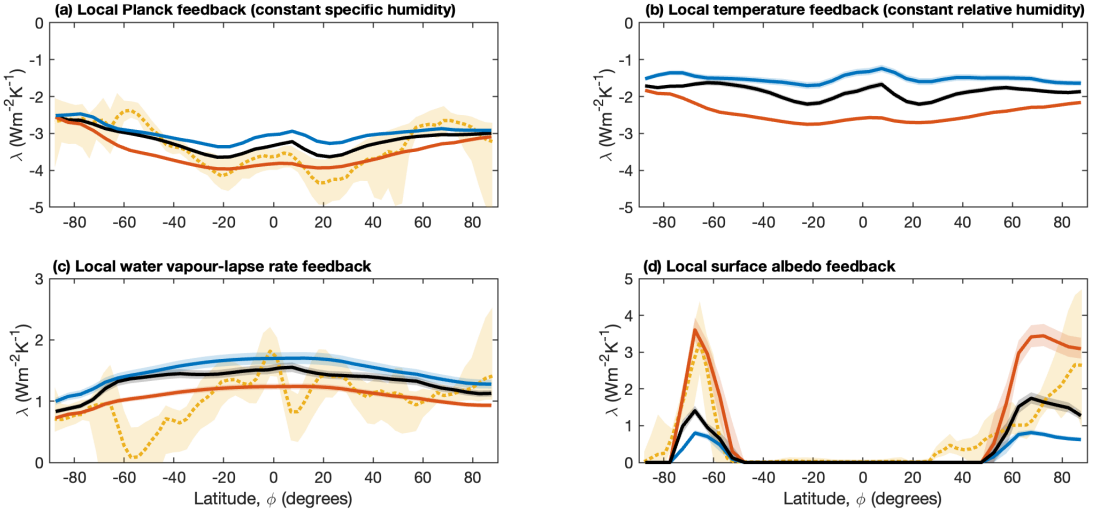

Figure 6: Annual and zonal-mean climate feedbacks with latitude evaluated from functional relationships and recent climatology. The (a) Planck feedback at constant specific humidity and (b) the temperature feedback at constant relative humidity, (c) the water vapour-lapse rate feedback and (d) the surface albedo feedback are given for all sky (black), clear sky (red) and cloudy sky (blue) conditions. Solid lines (median) and shading (17th to 83rd percentile) show evaluations from recent climatology and approximate functional relationships: black is for all-sky, blue is for cloudy-sky and red is for clear-sky conditions. For comparison, panels (a), (c) and (d) show the relevant climate feedback for the final 20-years of a 150-year abrupt 4xCO_2 perturbation experiment, a multi-model mean of 15 CMIP6 models, evaluated using a radiative kernel decomposition (Appendix A). Orange dotted lines show the multi-model mean and orange shading shows the range across the 15 models.

https://doi.org/10.5194/egusphere-2023-2307
Preprint. Discussion started: 24 October 2023

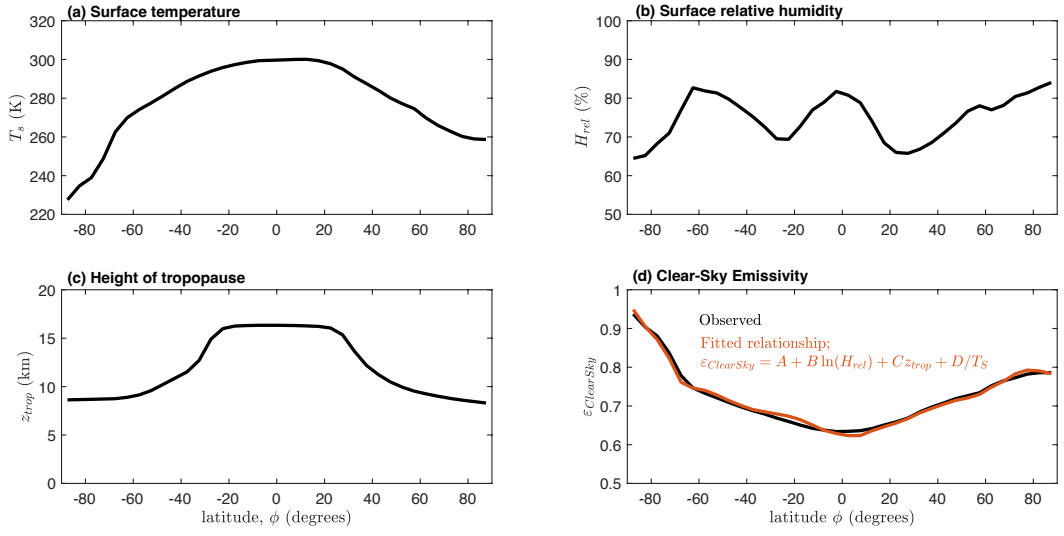

Figure 7: Annual- and zonal-mean climatological properties with latitude: (a) surface temperature, (b) surface relative humidity, (c) tropopause height, (d) clear-sky emissivity. Statistical model based on $\varepsilon_{ClearSky} \approx A + B \ln H_{rel} + Cz_{trop} + \frac{D}{T_S}$, eq. (17).

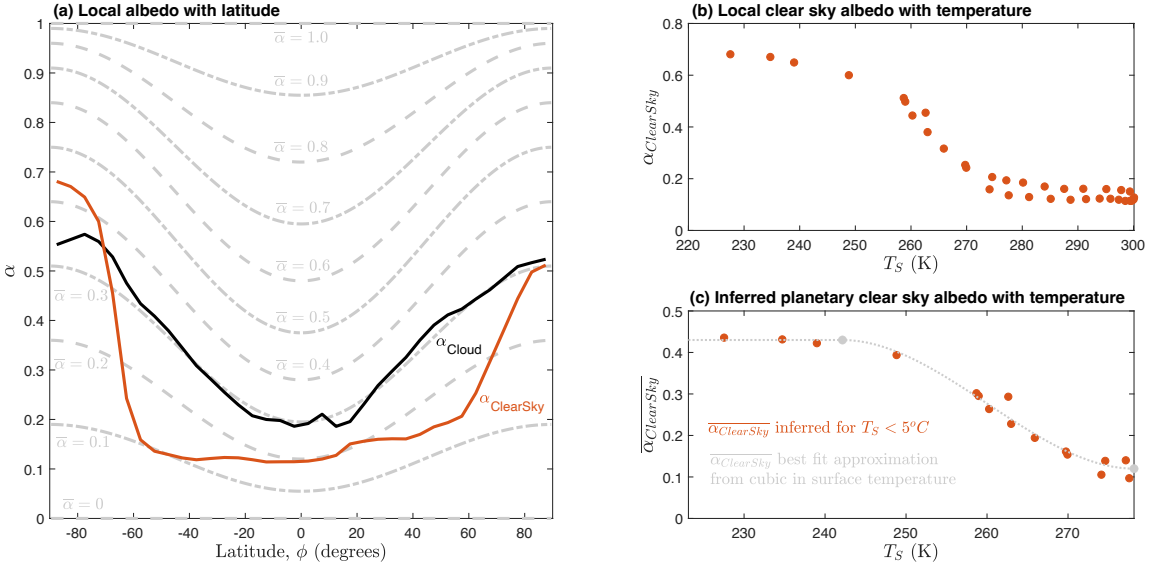

Figure 8: Albedo with latitude and temperature. (a) Annual- and zonal-mean albedo with latitude for clear-sky conditions (red), for cloud with directed solar radiation (black) and using the approximation $\bar{\alpha}[1 + [1 - \bar{\alpha}]P_2(\sin\phi)]$ for different values of global mean albedo $\bar{\alpha}$ (grey), where P_2 signifies the second order Legendre polynomial. (b) Local annual- and zonal-mean clear-sky albedo with annual- and zonal mean temperature. (c) Inferred planetary mean surface albedo, $\bar{\alpha}$, with annual- and zonal-mean surface temperature from observations (red) and a cubic approximation (grey).

https://doi.org/10.5194/egusphere-2023-2307
Preprint. Discussion started: 24 October 2023

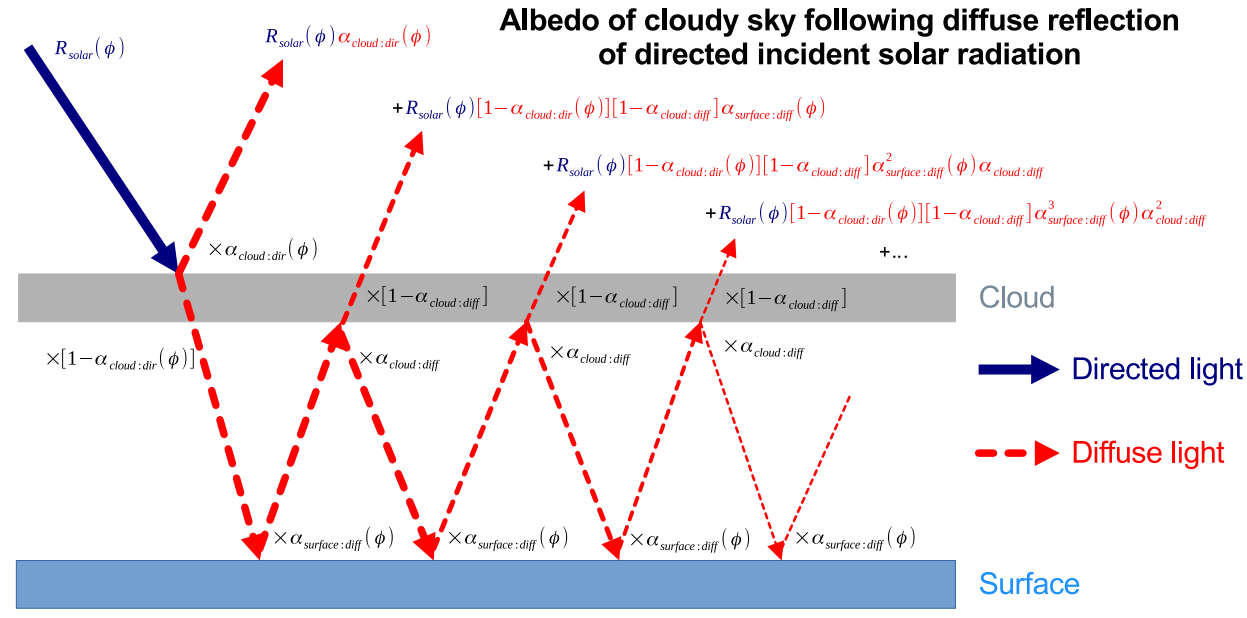

Albedo of cloudy sky = 'sum of outgoing radiation above cloud' / 'incident solar radiation'

$$\alpha_{CloudySky}(\phi)=\alpha_{cloud:dir}(\phi)+\alpha_{surface:diff}(\phi)[1-\alpha_{cloud:dir}(\phi)][1-\alpha_{cloud:diff}]\sum_{n=0}^{\infty}\alpha^n_{surface:diff}(\phi)\alpha^n_{cloud:diff}$$

$$\alpha_{CloudySky}(\phi)=\alpha_{cloud:dir}(\phi)+\alpha_{surface:diff}(\phi)\frac{[1-\alpha_{cloud:dir}(\phi)][1-\alpha_{cloud:diff}]}{[1-\alpha_{surface:diff}(\phi)\alpha_{cloud:diff}]}$$

Figure 9: Simplified model of albedo in cloudy sky conditions, with separate directed and diffuse shortwave beams.

https://doi.org/10.5194/egusphere-2023-2307
Preprint. Discussion started: 24 October 2023

Climate feedbacks ($Wm^{-2}K^{-1}$)	**This study, uniform warming** *{median, (66% range) [90% range]}*	**This study, patterned warming** *{median, (66% range) [90% range]}*	**AR6** *{median, (66% range) [90% range]}*	**Sherwood et al.** *{mean ± standard deviation}*	**CMIP6** *{mean ± standard deviation}*
Planck feedback (constant specific humidity), $\lambda_{Planck:specific}$	-3.32	-3.30	-3.22 (-3.1 to -3.3) [-3.0 to -3.4]	-3.20 ±0.04	-3.28±0.05
Temperature feedback (constant relative humidity), $\lambda_{T:relative}$	-1.92 (-1.85 to -1.98) [-1.80 to -2.03]	-1.93 (-1.86 to -1.99) [-1.81 to 2.04]			-1.91±0.03[a]
WVLR, λ_{WVLR}	1.41 (1.34 to 1.48) [1.29 to 1.53]	1.38 (1.31 to 1.45) [1.27 to 1.49]	1.30 (1.2 to 1.4) [1.1 to 1.5]	1.15 ± 0.15	1.33±0.09
Surface albedo, λ_{albedo}	0.21 (0.18 to 0.24) [0.16 to 0.26]	0.37 (0.34 to 0.40) [0.31 to 0.43]	0.35 (0.25 to 0.45) [0.10 to 0.60]	0.30 ± 0.15	0.45±0.09
Cloud feedback, λ_{Cloud}	-	-	0.42 (0.12 to 0.72) [0.10 to 0.94]	0.45 ± 0.33	0.42 ± 0.36
Total climate feedback, λ_{total}	-1.25[b] (-0.92 to -1.59) [-0.57 to -1.93]	-1.10[b] (-0.76 to -1.44) [-0.42 to -1.78]	-1.16 (-0.78 to -1.54) [-0.51 to -1.81]	-1.30 ± 0.44	-1.00 ± 0.34

Table 1: Climate feedback terms compared to IPCC Assessment and CMIP models. [a]CMIP6 values are the Planck feedback at constant relative humidity, without lapse rate adjustment. CMIP6 values taken from Zelinka et al. (2020). [b]Combines Planck, WVLR and albedo feedbacks with Sherwood et al. (2020) estimate for cloud feedback.

Coeff.	**Estimate**	**Standard Error**	**t-statistic**	**p-value**
A	0.272	0.122	2.22	0.0337
B	−0.0897	0.0212	−4.24	0.0001792
C (km^{-1})	−0.00329	0.00089	−3.70	0.000816
D (K)	242.96	10.01	24.27	3.55×10^{-22}

Table 2: Statistical model fit for $\varepsilon_{ClearSky} \approx A + B \ln H_{rel} + Cz_{trop} + \frac{D}{T_S}$ using recent climatology. Number of observations = 36; Error degrees of freedom = 32; Root Mean Squared Error = 0.00822; $R^2 = 0.99$; Adjusted $R^2 = 0.989$; F-statistic vs. constant model: 1.04×10^3; p-value = 5.69×10^{-32}.